Utah State University

DigitalCommons@USU

5-2011

A Linearly and Circularly Polarized Active Integrated Antenna

Ali Khoshniat

Utah State University

A LINEARLY AND CIRCULARLY POLARIZED

ACTIVE INTEGRATED ANTENNA

by

Ali Khoshniat

A thesis submitted in partial fulfillment
of the requirements for the degree

of

MASTER OF SCIENCE

in

Electrical Engineering

Approved:

<table>
<tr><td>_____</td><td>_____</td></tr>
<tr><td>Dr. Reyhan Baktur
Major Professor</td><td>Dr. Doran Baker
Committee Member</td></tr>
<tr><td></td><td></td></tr>
<tr><td>_____</td><td>_____</td></tr>
<tr><td>Dr. Jacob Gunther
Committee Member</td><td>Dr. Byron R. Burnham
Dean of Graduate Studies</td></tr>
</table>

UTAH STATE UNIVERSITY
Logan, Utah

2011

Abstract

A Linearly and Circularly Polarized

Active Integrated Antenna

by

Ali Khoshniat, Master of Science

Utah State University, 2011

Major Professor: Dr. Reyhan Baktur
Department: Electrical and Computer Engineering

This thesis work presents a new harmonic suppression technique for microstrip patch antennas. Harmonic suppression in active integrated antennas is known as an effective method to improve the efficiency of amplifiers in transmitter side. In the proposed design, the antenna works as the radiating element and, at the same time, as the tuning load for the amplifier circuit that is directly matched to the antenna. The proposed active antenna architecture is easy to fabricate and is symmetric, so it can be conveniently mass-produced and designed to have circular polarization, which is preferred in many applications such as satellite communications.

The antenna simulations were performed using Ansoft High Frequency System Simulator (HFSS) and all amplifier design steps were simulated by Advanced Design System (ADS). The final prototypes of the linearly polarized active integrated antenna and the circularly polarized active integrated antenna were fabricated using a circuit board milling machine. The antenna radiation pattern was measured inside Utah State University's anechoic chamber and the results were satisfactory. Power measurements for the amplifiers'

performance were carried out inside the chamber and calculated by using the Friis transmission equation. It is seen that a significant improvement in the efficiency is achieved compared to the reference antenna without harmonic suppression.

Based on the success in the single element active antenna design, the thesis also presents a feasibility of applying the active integrated antenna in array configuration, in particular, in scanning array design to yield a low-profile, low-cost alternative to the parabolic antenna transmitter of satellite communication systems.

(80 pages)

To my beloved wife...

Acknowledgments

First of all, I would like to thank my advisor, Dr. Reyhan Baktur, for the opportunity of working in her research group and on this project. This thesis work would have never been completed without her guidance, patience, and expertise in the field of antenna and microwave circuits. I also want to thank her for the time and effort in reviewing and giving me feedback about my work.

I would also like to acknowledge other members of my committee, Dr. Doran Baker and Dr. Jacob Gunther, for their time in helping this thesis become a better product. I would like to thank the ECE department head, Dr. Todd Moon, for being very supportive to me pursuing my MS degree. I also want to thank the ECE store coordinator, Heidi Harper, for purchasing the components and providing the measurement equipment. I want to thank my colleague at Utah State University, Tursunjan Yasin, for our long discussions about this project.

I want to thank all my friends in Logan for the great time I had with them. Finally, I would like to thank my wife, Maryam. I could not have finished my program without her support.

Ali Khoshniat

Contents

List of Figures

Chapter 1

Introduction

Wireless communication systems have been seeking a compact and low-cost transmitter front-end without sacrificing system performance. Crucial factors for wireless transmitters include efficiency, size, and bandwidth [1]. Power Amplifiers (PAs) are the most power-consuming components in transmitter designs; therefore, improving the efficiency of PAs is an important issue for wireless communication systems. Even a few percent of improvement in Power Added Efficiency (PAE) can be significant if it can be designed without major degradation in linearity [2].

In microwave networks, there are two different definitions for PAE [3]. The first definition is generic to all multiple-port networks and is the ratio of the total output power to the total input power (1.1). The second definition is specific to the Radio Frequency (RF) power amplifiers and is widely regarded as the industry standard (1.2). In these equations P_{IN} represents input power, P_{OUT} represents output power, and P_{DC} is the total DC power. There is a slight difference between the calculated PAE using each definition. In this work, we adopt the first definition.

$$\eta = \frac{P_{OUT}}{P_{IN} + P_{DC}} \times 100\,\% \tag{1.1}$$

$$\eta = \frac{P_{OUT} - P_{IN}}{P_{DC}} \times 100\,\% \tag{1.2}$$

The Active Integrated Antenna (AIA) can be regarded as an active microwave circuit in which the output or input port is free space instead of a conventional 50-ohm interface. The antenna is not only used as a radiating element, but also provides certain circuit functions such as resonating, filtering, and diplexing, and is an integral part of the microwave circuit

design [4].

In power amplifier design, such integration not only offers a compact size for RF front-ends, but also enables higher PAE for the PA. Traditional amplifier design generally matches the output of a PA to a 50-ohm transmission line, and then the line is matched to an antenna. In AIA design, however, the antenna serves as the load for the PA and there is only one matching network between them. Therefore, AIA has a relatively compact size. It has been shown that suppressing higher harmonics of a PA helps to improve PAE [2, 4–7]. In push-pull topology as another configuration for amplifiers, the antenna can work as power combiner as well as radiating element and this can enhance PAE [5,8–11]. Other applications of AIA are in receivers to improve the Noise Figure (NF) [5], in rectenna design [12], in integrated antenna oscillators [2], in compact transmitter and receiver systems [2], and in Retro Directive Array (RDA) systems [5]. In our work we are interested in integration of amplifier and antenna to improve PAE in a transmitting module. Therefore, following [2, 4–7], our approach is to design a multifunctional antenna, where the antenna is the radiating element as well as the harmonic suppressing load for the amplifier.

An antenna which supports linear (vertical and horizontal) and circular (right-hand and left-hand) polarizations is suitable for satellite communication applications, therefore, our target is to design the antenna supporting all different types of polarizations. An array of these active elements can be an alternative for conventional parabolic antennas by providing good directivity while the weight and cost of production for a planar antenna is less when compared with a parabolic antenna having the same specifications.

One possible application for the designed antenna is in Ku band satcom links where the uplink allocated bandwidth is $12.75 - 14.5\,GHz$ and the downlink allocated bandwidth is $11.7 - 12.7\,GHz$. As we are designing the ground station, the frequency should be in the uplink bandwidth for our antenna and amplifier. In this work, as we want to prove the antenna and amplifier performance, we have selected a frequency which is suitable for our fabrication and antenna measurement facility. The selected frequency is $2.4\,GHz$ and we plan to have $10\,mW$ output for the amplifier which is desired for the final design.

This thesis is organized as follows: first, design of the microwave amplifier is described; next, the antenna design and harmonic suppression method is explained; and finally, the antenna integration with the amplifier and the measurement results for linearly and circularly polarized active integrated antennas are presented.

Chapter 2

Microwave Power Amplifiers – Background and Test Design

Microwave amplifiers are categorized based on their characteristics such as linearity, efficiency, output power, and signal gain. In general, there is always a tradeoff between them [13] and the most critical parameter depends on specific application. For example, in the transmitter side the efficiency is critical, while on the receiver side the most important characteristic is linearity. The purpose of this thesis research is to provide an effective AIA for the transmitter side, and accordingly the selection of the PA specifications is determined to fit this target application.

2.1 Amplifier Classes of Operation

A brief summary about the amplifiers class of operation from Bahl [14], helps increase understanding of this chapter. In an amplifier design, the bias condition known as Quiescent point (Q-point), the source impedance, and the load impedance for maximum power delivery should be considered. These three requirements determine NF, gain, bandwidth, output power, PAE, and linearity in performance of the amplifier in its operation. At RF/microwave frequencies the amplifiers are mainly categorized in these classes: A, B, AB, C, D, E, and F. These classes are implemented by assigning the appropriate Q-point and providing the matching conditions for input and output ports of the active element. The amplifier's performance and its characteristics in each class are briefly described in the following sections and the details could be found in Bahl [14]. All the definitions below are for Field Effect Transistors (FET) but simply could be mapped to Bipolar Junction Transistors (BJT) or other types as well.

2.1.1 Class A Amplifier

In class A, the amplifier is conducting the sinusoidal signal in a full cycle of 360 degrees. That means the Q-point is almost at the center of the device current and the output signal has its maximum linearity. The maximum drain efficiency of a class A amplifier is 50%. Assuming that there is no saturation and the device is working in the linear portion of its transfer function, then the input and output waveforms of the signals are the same [14].

2.1.2 Class B Amplifier

In class B, the Q-point is set at the cutoff of the device current and that means the amplifier conducts only a half cycle (180 degrees) of the sinusoidal input signal and it is almost off (with negligible current) in the other half cycle. So the linearity of output signals is poor compared to class A. Theoretically class B amplifiers have maximum 78.5% drain efficiency [14]. In this project, as we are interested in high efficiency but do not want much linearity, the class B amplifier is chosen. However, the same study could be done for other types of amplifiers based on the application requirements.

2.1.3 Class AB Amplifier

In class AB, the device Q-point is between class A and Class B between $5 - 30\%$ of the total device current. The efficiency in this class is not as high as class B but there is an improvement in the linearity [14].

2.1.4 Class C Amplifier

In class C, the Q-point is set bellow the cutoff point of the transistor current and the device conducts over $25 - 45\%$ of the RF cycle. This amplifier is very nonlinear but the efficiency is higher than class A, B, or AB. This type of device is used in the applications where linearity is not required [14].

2.1.5 Class D, E, and F Amplifiers

In these classes, the transistor works as a switch with very low resistance in the "ON

state and very high impedance in the "OFF state. So in the "ON state there is no power dissipation in the device and in the "OFF state there no current consumption. In the ideal switching the efficiency is 100% but in reality as the above assumption is not correct, the efficiency would be less but still better than class A, B, AB, and C. In class D there is no tuned circuit as the load for the amplifier but in class E and F the load could work as a high Q tuned circuit to take fundamental frequency of the pulsed output and in that way the output signal would be similar to a sinusoidal wave [14].

2.2 Microwave Power Amplifier Design

The most important design considerations in a microwave amplifier are stability, power gain, bandwidth, noise, and DC requirements. After deciding about the specifications, the next step is to select the proper transistor based on the requirements. With some simplifications in the equations and by using the S-parameter model of the transistor, one can design an amplifier following the method described in the following sections. Although there is always need for optimization of the initial design after the first simulation, these formulas are good enough to start the design. More details for equations and design procedure are available in references [15, 16].

2.2.1 Power Gain Equations

Several power gain equations appear in the literature and are used in the microwave amplifier design. The transducer power gain G_T (2.1), the power gain G_P (2.2), and the available power gain G_A (2.3) are defined as follows:

$$G_T = \frac{power\ delivered\ to\ the\ load}{power\ available\ from\ the\ source}, \tag{2.1}$$

$$G_P = \frac{power\ delivered\ to\ the\ load}{power\ input\ to\ the\ network}, \tag{2.2}$$

$$G_A = \frac{power\ available\ from\ the\ network}{power\ available\ from\ the\ source}. \tag{2.3}$$

In the design of an amplifier which we assume that we know the S-parameters of the transistor, we are interested in finding transducer power gain. For most of the transistors S_{12} is close to zero and we can consider the network to be unilateral. In that case the simplified equation to calculate unilateral transducer power gain G_{TU} is (2.4) where Γ_S is the reflection coefficient seen looking toward the source, Γ_L is the reflection coefficient seen looking toward the load, and S_{11}, S_{21}, and S_{22} are S-parameters of the transistor at the desired frequency.

$$G_{TU} = \frac{1 - |\Gamma_S|^2}{|1 - S_{11}\,\Gamma_S|^2}\ |S_{21}|^2\ \frac{1 - |\Gamma_L|^2}{|1 - S_{22}\,\Gamma_L|^2} \tag{2.4}$$

Equation (2.4) can be understood to be composed of three distinct and independent gain terms in the form of (2.5) where G_S, G_0, and G_L are defined in (2.6), (2.7), and (2.8).

$$G_{TU} = G_S \times G_0 \times G_L \tag{2.5}$$

$$G_S = \frac{1 - |\Gamma_S|^2}{|1 - S_{11}\,\Gamma_S|^2} \tag{2.6}$$

$$G_0 = |S_{21}|^2 \tag{2.7}$$

$$G_L = \frac{1 - |\Gamma_L|^2}{|1 - S_{22}\,\Gamma_L|^2} \tag{2.8}$$

Following the steps, the microwave amplifier can be represented by three different gain blocks as shown in Fig. 2.1 and to get the maximum unilateral transducer power gain, G_S and G_L should be maximized under the conjugate matching conditions in (2.9) and (2.10).

$$\Gamma_S = S_{11}^* \tag{2.9}$$
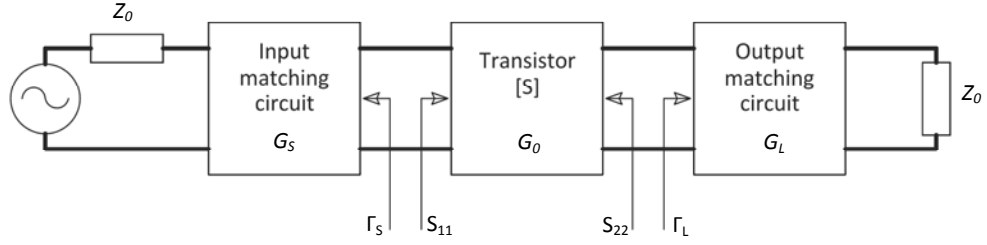
Fig. 2.1: Block diagram of a microwave amplifier to find unilateral transducer power gain.

$$\Gamma_L = S_{22}^* \tag{2.10}$$

The design procedure starts by considering the transistor's S-parameters at the desired frequency. By assuming the device as a unilateral network and using (2.9) and (2.10), the last step is to design two matching networks to be connected to the source and the load. Because we assume that the transistor is unilateral to simplify the design equations, in the real case we will see some differences between the results of simulation and our expectations because the transistor is actually bilateral. Some optimization is needed during the simulation to tune the matching networks for the best response.

2.2.2 Stability Considerations

The stability of an amplifier is defined as its impervious to oscillate [15]. Oscillations are possible to happen when the input or output port presents a negative resistance. If we consider the amplifier as a two-port network shown in Fig. 2.2, oscillation can occur if $|\Gamma_{IN}| > 1$ or $|\Gamma_{OUT}| > 1$.

There are two types of stability defined for two-port microwave networks: unconditional stability and conditional stability. The network is unconditionally stable if $|\Gamma_{IN}| < 1$ and $|\Gamma_{OUT}| < 1$ are satisfied for all passive source and load impedances. The network is conditionally stable if $|\Gamma_{IN}| < 1$ and $|\Gamma_{OUT}| < 1$ are satisfied only for a certain range of passive source and load impedances. This case is also referred to as potentially unstable.
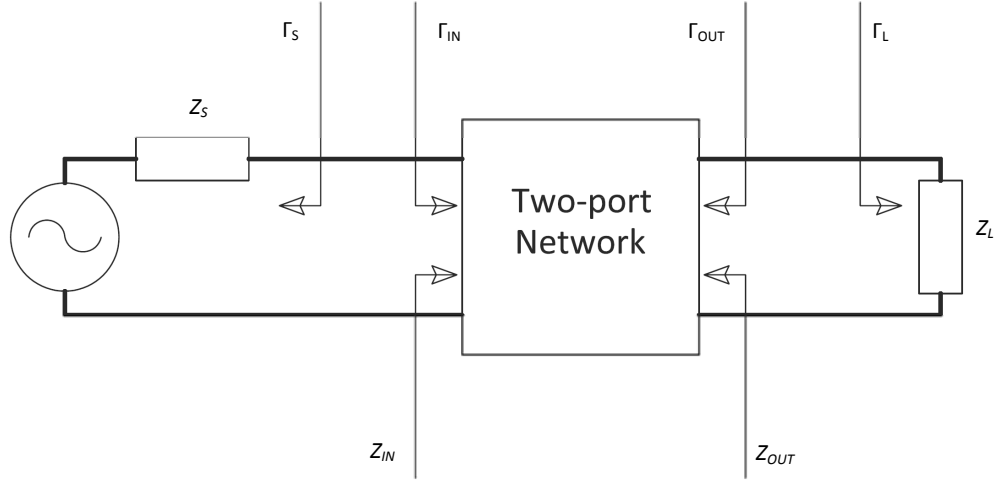
Fig. 2.2: Stability of two-port network.

The necessary and sufficient conditions for unconditional stability are given as (2.11) and (2.12) where Δ is defined as (2.13).

$$K = \frac{1 - |S_{11}|^2 - |S_{22}|^2 + |\Delta|^2}{2\,|S_{12}\,S_{21}|} > 1 \tag{2.11}$$

$$B_1 = 1 + |S_{11}|^2 - |S_{22}|^2 - |\Delta|^2 > 0 \tag{2.12}$$

$$|\Delta| = |S_{11}\,S_{22} - S_{12}\,S_{21}| \tag{2.13}$$

2.2.3   Direct Current (DC) Bias Circuit

After designing the matching networks for input and output ports providing maximum gain while considering the amplifier's stability, the next part is DC bias circuit. This circuit should be able to isolate the RF sections of the amplifier from the DC parts. It should be also able to deliver the required DC power with minimum dissipation as we are interested in an efficient design. The isolation can be done using Radio Frequency Choke (RFC) as a lumped element in low frequencies or using a piece of transmission line printed on the

circuit as an inductor. The width of this transmission line should be very narrow to increase its characteristic impedance and the length should be quarter wavelength at the frequency of the amplifier's operation.

This quarter wavelength transmission line is directly connected to the input or output ports of the transistor and its relatively high impedance compared to other parts of the matching network makes its effect as small as possible. On the other side of this narrow transmission line where the DC supply is connected, using some decoupling capacitors effectively short circuits all frequencies except the DC supply at that point. The quarter wavelength transmission line will transform the short circuit to an open circuit where it is connected to the amplifier's network. That means the input or output signals cannot propagate inside that part of the circuit and in this way the RF network is isolated from the DC circuit. Simplified schematic for RF and DC sections are illustrated in Fig. 2.3.

Finally, DC voltage and current for the transistor at its operation determine the intended class of amplifier. As described before in the amplifier classes, knowing the DC voltage and current at the Q-point and by considering the transistor's characteristics, the appropriate supply voltage should be assigned to drive the amplifier.
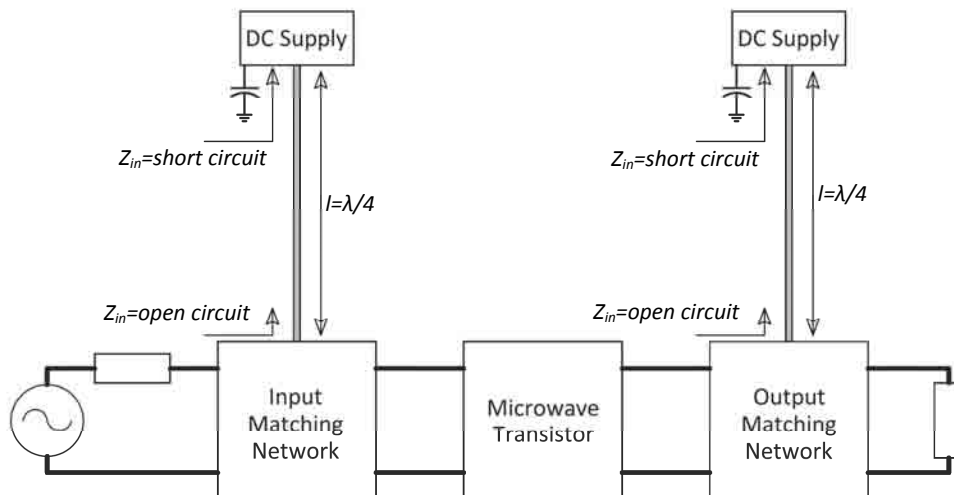
Fig. 2.3: DC circuit for microwave amplifier.

2.2.4   Power Amplifier Design Considerations

Power amplifiers are normally used as the final stage of the circuit in the RF transmitters. The power level may be in the order of $100 - 500\,mW$ for mobile communications systems or range of $1 - 100\,W$ for radar or fixed point radio systems. The important considerations for RF and microwave power amplifiers are efficiency, gain, intermodulation products, and thermal effects.

As we discussed about amplifier design before, all the time we assumed that the input signal power is small enough that the amplifier is working as a linear device. In that case the S-parameter model of the transistor is fixed and is not dependent on the power level of the input signal. For high input powers in the range of $1\,dB$ compression point, the transistor do not behave linearly and in that case the impedance seen at the input and output of the transistor will depend on the input power level, and this greatly complicates the design of power amplifiers although there are some nonlinear models developed for power amplifiers which could be used in the simulation to help the designers in this process.

2.3   The Design of Amplifier at 2.4 GHz

As discussed in Chapter 1, the prototype for the amplifier should be in class B working at $2.4GHz$ with minimum $10dBm$ output power. The selected transistor was NESG2031M16 manufactured by California Eastern Laboratories (CEL) [17]. All design steps for matching networks, stability, and DC biasing were done using schematic wizard of Advanced Design System (ADS) by Agilent Technologies [18] using the model provided by CEL for that transistor. The amplifier was designed on RO4003C substrate with $32\,mil$ thickness provided by Rogers Corporation [19] and the final optimized AutoCAD [20] layout is given in Fig. 2.4 showing the lumped elements such as capacitors and resistors and the transistor's position.

The input and output ports are matched to 50-ohm transmission line which is a microstrip line with $1.8\,mm$ width. Some pads should be grounded and therefore there are some connections to the reference ground plane using via that is shown in the layout with dark gray circles. The conductive connections inside these holes are made by punching some metallic bars in the holes and soldering them to each face of the board. The transistor shown
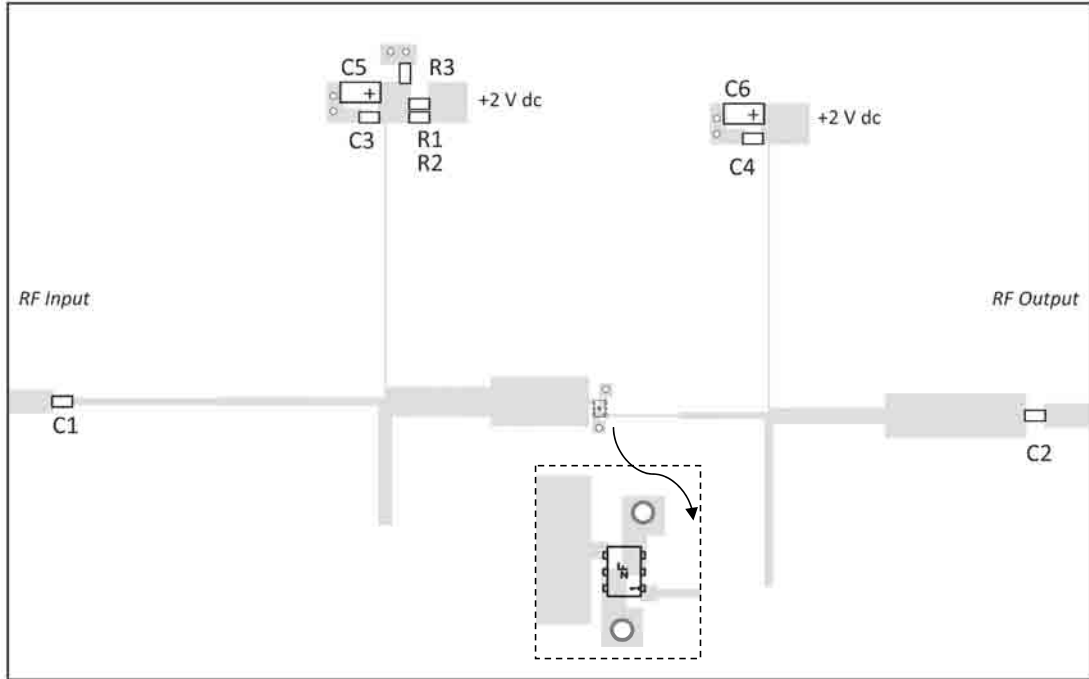
Fig. 2.4: Layout of $2.4\,GHz$ amplifier.

with name "zF is NESG2031M16 with six pins and overall size of $1.2\,mm$ by $1\,mm$. The values for other lumped elements are: $C1, C2 = 10\,pF$, $C3, C4 = 10\,nF$, $C5, C6 = 10\,\mu F$ using Tantalum capacitors for stabilizing DC voltage, $R1 = 12\,k\Omega$, $R2 = 27\,k\Omega$, and $R3 = 56\,k\Omega$. All these components are Surface Mount Devices (SMD) with size 0603 except the Tantalum capacitors with size 1206. Figure 2.5 shows S-parameters of the amplifier from small signal simulation in ADS. Harmonic Balance (HB) simulation is needed to find output power and PAE at a certain frequency considering the harmonics of the signal as well as DC bias conditions. The results of HB simulation are shown in the next section in the same plot with the measurement to facilitate comparisons.

2.4 Fabrication and Measured Results

The designed amplifier layout was fabricated on the RO4003C substrate using the milling machine. As the transistor is very small in size and sensitive to the high temperature during soldering, we decided to use conductive epoxy H20E provided by Epoxy Technology
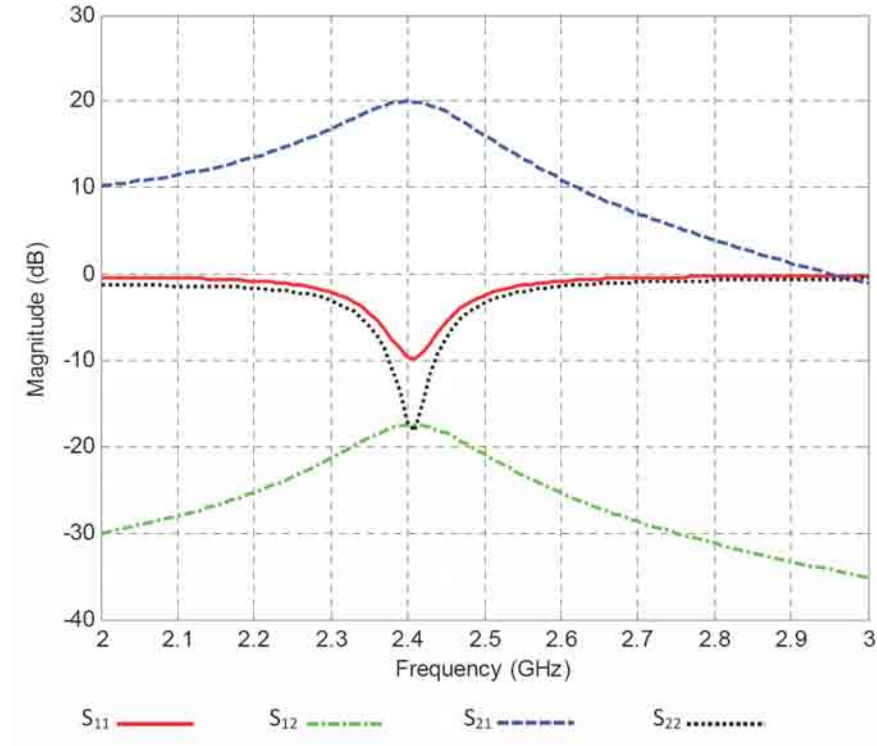
Fig. 2.5: S-parameter simulation results of the 2.4 GHz amplifier.

[21] to attach the transistor to the circuit electrically and mechanically. This type of epoxy has two components needed to be mixed with the same weight ratio and then it could be used as glue. It is not conductive at the time of mixing and needs curing in a way described in the datasheet to make it a good conductor as well as a solid material so we used an oven for this reason. After that, other elements like capacitors and resistors were soldered in a conventional way using iron and soldering wire, and finally two SubMiniature version A (SMA) connectors were connected as the 50-ohm ports. Figure 2.6 shows the fabricated amplifier at 2.4 GHz and the tiny transistor is located at the center of the circuit. The wire is used for positive DC connection and the ground for DC and RF are common as the reference ground plane on the other side of the substrate. Input and output ports are indicated in the figure as well.

The measurement setup consists of a RF signal source to provide different input power levels at a the measurement frequency which is 2.4 GHz in our application, spectrum ana-
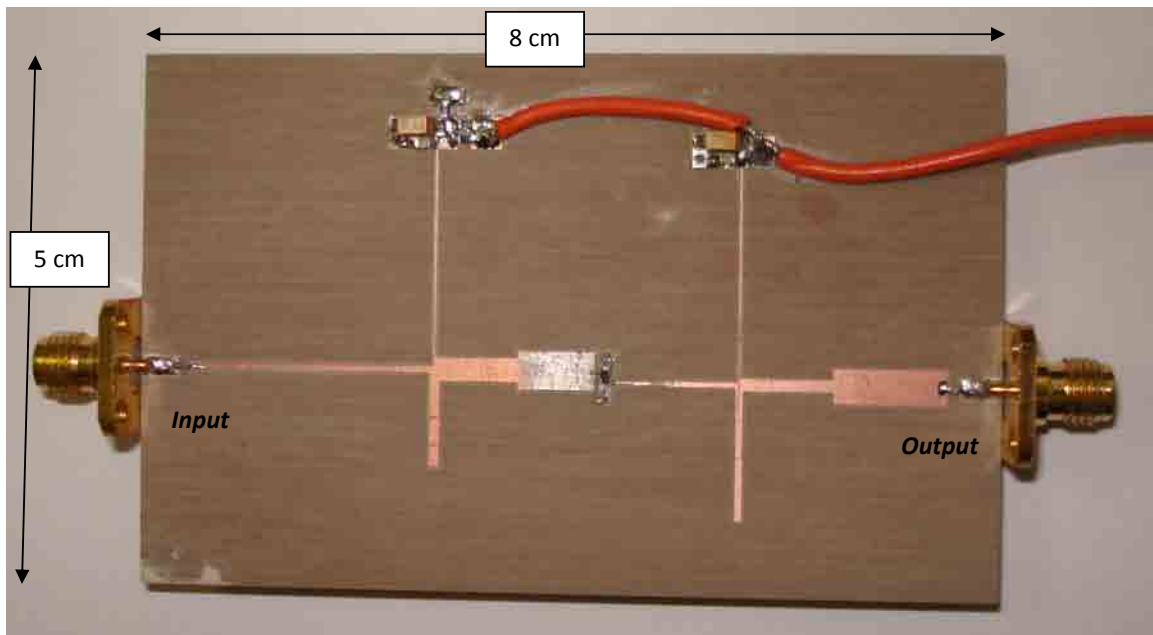
Fig. 2.6: Fabricated amplifier at $2.4\,GHz$.

lyzer to measure the output power level for different input power levels, DC power supply providing $+2\,V\,DC$, and a digital multi-meter to measure DC voltage and current to calculate total DC input power for the amplifier. We performed the measurement for output power at different power levels of RF input signal. Figure 2.7 shows simulation and measurement results of the amplifier output power versus input power level.

To calculate PAE using (1.1), we need the measured output RF power and input DC power for different input RF power levels. The simulation and measurement results of PAE for the amplifier are given in Fig. 2.8. As we can see, there is a good agreement between the results of simulation and measurement for both output power and PAE.

These simulation and measurement results assure that our amplifier design method is correct and we can use the same transistor for the amplifier design later.
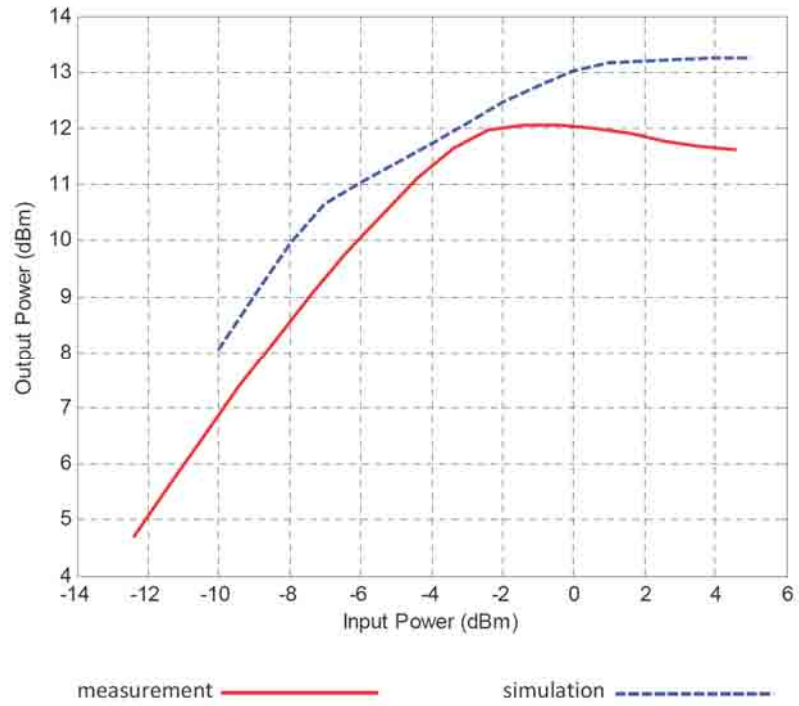
Fig. 2.7: Simulated and measured output power of the 2.4 GHz amplifier.
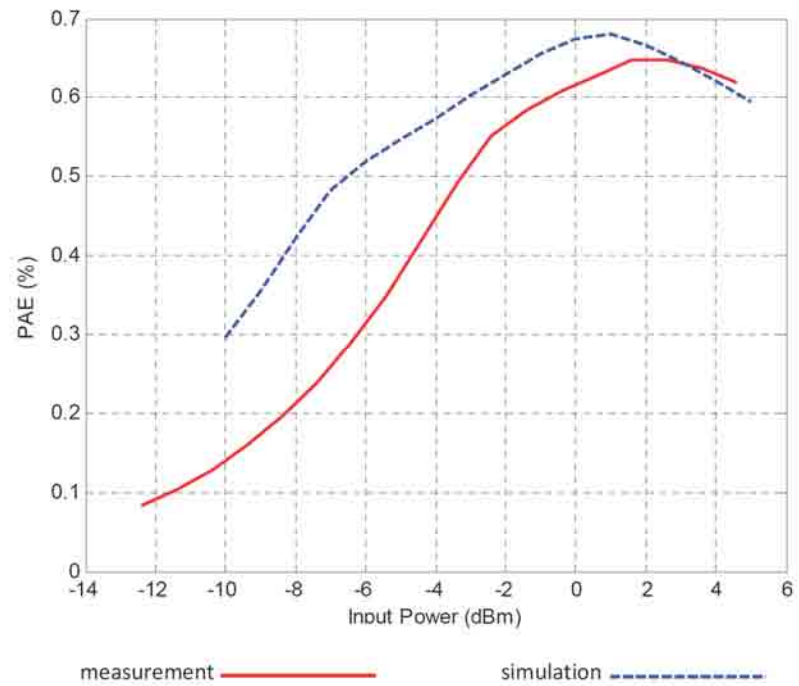
Fig. 2.8: Simulated and measured PAE of the 2.4 GHz amplifier.

Chapter 3

Antenna Design

3.1 Harmonic Suppression

As explained in Chapter 1, when the antenna is directly connected to the output of an amplifier it also works as the load for that circuit. This frequency dependent load could be tuned at the amplifier's frequency of operation for improving the matching to maximize power delivery to the antenna [6, 22, 23]. There is more improvement in the efficiency if the antenna input impedance at the amplifier's harmonics provide great mismatch to suppress them. This could be presented with ideally $|\Gamma| = 0$ at the fundamental frequency and $|\Gamma| = 1$ at the harmonics. Looking at S_{11} in dB for the antenna, it should be smaller than $-10\,dB$ at the fundamental frequency and larger than $-1\,dB$ very close to $0\,dB$ at the harmonics.

The other method for harmonic suppression, which will result in the same manner of harmonic suppression for the amplifier, is to make the input impedance of the antenna at the harmonics either very close to zero or very large [6, 7, 24]. This will assure that there is enough reflection at the harmonics to suppress them. Although it is sufficient just to make the real part of the input impedance close to zero as it makes the load to be reactive which means there would not be any power consumption for those harmonic frequencies [24].

Explained definitions for the harmonic suppression in antennas, reflection measurement and input impedance consideration, have the same result for amplifier's performance in active circuits. As reflection is defined for transition between two impedances (mostly the reference impedance is 50 ohm), and in this work the amplifier and the antenna are not necessarily 50 ohm, input impedance of the antenna is considered as a factor of indication for the harmonic suppression.

3.2 Harmonic Suppression Techniques for Planar Antennas

There have been several successful techniques in the literature to suppress harmonics of a planar antenna. Typical methods include using shorting pins to suppress the second harmonic in the rectangular patch [1, 25, 26], cutting off some pieces of the patch like a circular sector antenna to move the second and third harmonics resonances from their original frequencies [1, 27–29], and combination of these two methods in a rectangular patch with some slits while using a shorting pin [30]. Using slot coupling for patch excitation while cutting some parts in a H-shaped patch is reported as another method for harmonic suppression [31]. Other architectures such as ground periodic structure [1], Photonic Band Gap (PBG) structure [32–37], and defected ground structure [38] are also effective in harmonic suppression by changing the ground plane for the patch or the transmission line. There are a few methods for slot antennas, where the harmonics are suppressed by making certain changes in the shape of the slot near the feed area or making a meandered slot and so on [6, 7, 23, 24, 39].

3.3 Design Background

Microstrip patch antennas are very conventional in wireless communications because of their low profile geometry, easy fabrication, and their capability to be integrated with RF circuits. Rectangular patch is one common structure and we are interested to use it in our application.

There are two models to analyze the behavior of one patch antenna based on its dimensions and the substrate properties. It could be modeled as a transmission line or a cavity and as explained in references [40–43]. There are design equations to express the relation between patch length and resonance frequency, the width and optimum performance of the patch, and all are based on the substrate material and its thickness.

For a simple rectangular patch as illustrated in Fig. 3.1 with the shown dimensions, the resonance frequency f_r only depends on the length of the patch L and can be calculated using (3.1) where c_0 is the speed of light and L_{eff} and ε_e are defined in (3.2) and (3.3).
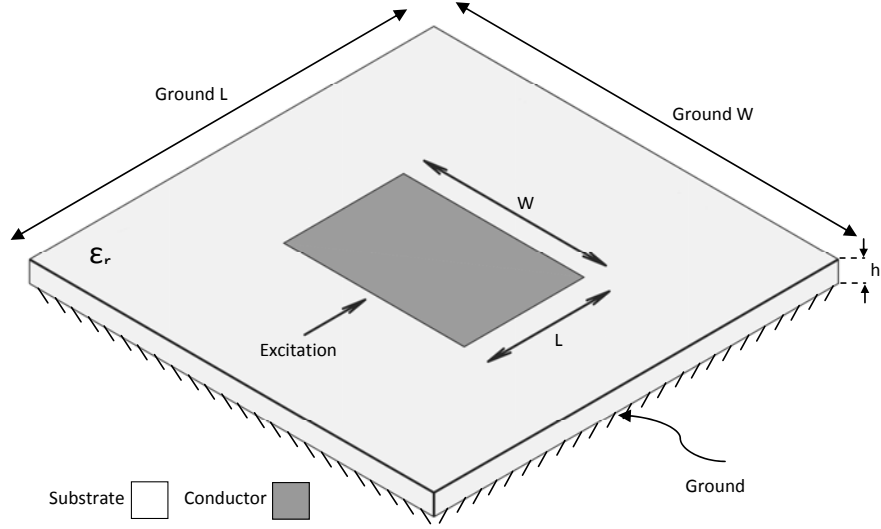
Fig. 3.1: Simple rectangular patch and the dimensions.

$$f_r = \frac{c_0}{2 \, L_{eff} \, \sqrt{\varepsilon_e}} \tag{3.1}$$

$$L_{eff} = L \, \left\{ 1 + 0.824 \, \frac{h}{L} \, \frac{(\varepsilon_e + 0.3) \left(\frac{L}{h} + 0.262 \right)}{(\varepsilon_e - 0.258) \left(\frac{L}{h} + 0.813 \right)} \right\} \tag{3.2}$$

$$\varepsilon_e = \frac{\varepsilon_r + 1}{2} + \frac{\varepsilon_r - 1}{2} \left(1 + 12 \, \frac{h}{L} \right)^{-\frac{1}{2}} \tag{3.3}$$

The patch width W affects the input impedance of the antenna and its directivity. The optimum value for good radiation efficiency can be calculated using (3.4). Smaller width will result in reduced radiation efficiency and higher input impedance. As an example, to compare a rectangular patch with a square patch at the same frequency on the same substrate, the rectangular patch has 210 ohm input impedance and 75% radiation efficiency while the square patch input impedance is 290 ohm and its radiation efficiency is 70.5%. Application for the square patch antenna is later explained for circular polarization.

$$W = \frac{c_0}{2\,f_r}\sqrt{\frac{2}{\varepsilon_r + 1}} \tag{3.4}$$

The patch can be excited using different structures for the feed line; microstrip line feed, probe feed, aperture-coupled feed, and proximity-coupled feed are described in Balanis [40] and Bancroft [43]. More feed structures like feed through a gap, side-coupled microstrip feed, and double-layered closed type of feed mechanism in microstrip antennas are explained in Bhartia [42] and their properties and applications are expressed in more details.

The ground plane which is placed under the patch is assumed to have infinite size, but in reality the ground size is limited. This finite ground has some effects on the antenna parameters and its performance. If we increase the ground plane dimensions, after passing a certain size we can see the change in the results are negligible and we can consider that ground plane almost as an infinite one. A simple simulation on the effect of the ground plane size for a patch antenna is done using Ansoft High Frequency System Simulator (HFSS) provided by ANSYS [44]. In this study the ground dimensions are $Ground\,L$ and $Ground\,W$ as indicated in Fig. 3.1. We can relate the ground size to the wavelength of the antenna frequency of operation using $Ground\,L = L + 2 \times d$ and $Ground\,W = W + 2 \times d$ where d is changing from $0.05\,\lambda$ to $0.3\,\lambda$ and the plots for directivity of the antenna for all these ground planes are shown in Fig. 3.2. We can see that changing d from $0.2\,\lambda$ to $0.3\,\lambda$ is not changing behavior of the antenna in its maximum directivity while having a smaller back lobe that means this ground size is optimum. Although sometimes there are size limitations from the system aspect and the ground size could not be that big anyway.

Input impedance of a patch varies based on the feed structure and its position. In probe feeding it could be some values close to 50 ohm or higher values like a couple of hundred ohms. For the microstrip line feed the input impedance is defined right at the edge of the patch so it would be only dependent on the patch properties. The microstrip feed line can be analyzed separately as a piece of transmission line with known characteristic impedance. This input impedance, as shown in Fig. 3.3, has real part and imaginary part and the antenna is resonating at the frequency where the imaginary part is zero and the real
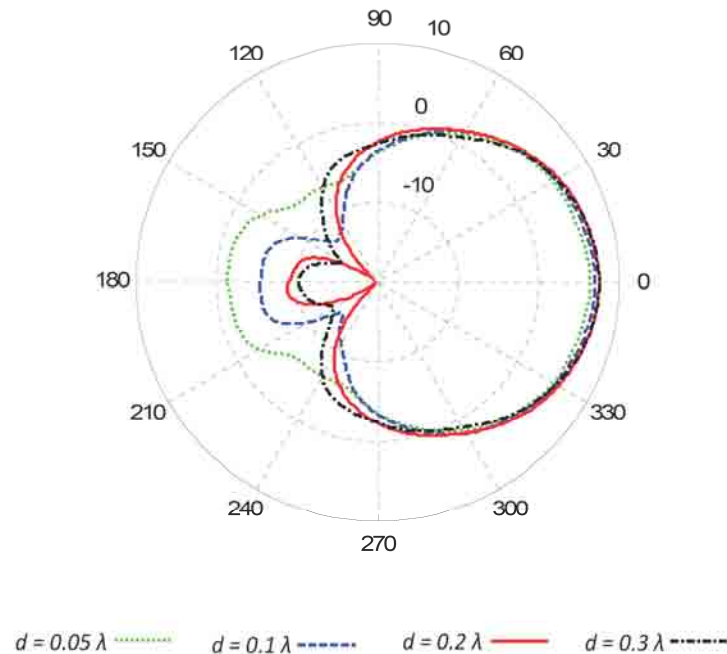
Fig. 3.2: The effect of ground size on the patch directivity.

part is at its maximum value. The equations for input impedance calculation and also other properties of the patch antennas like directivity, quality factor, bandwidth, and efficiency are explained in details in Balanis [40] and Hirasawa and Haneishi [41].

As discussed in Chapter 1, the final antenna should be designed for satellite communications supporting all possible polarizations. The best choice for this application is a square patch with two input ports. The schematic diagram for the top view for this antenna is shown in Fig. 3.4. By exciting port 1, the antenna works as a single patch with Linear Polarization (LP). Vertical or horizontal polarization is defined based on the positioning of the patch on the transmitter. If we assume that the antenna has vertical polarization when port 1 is active, using port 2 for excitation results in the horizontal polarization. As the patch is square, the resonance frequencies for these two excitations are the same, and the only difference is in the polarization. From the definition of Circular Polarization (CP) in Balanis [40] and Bancroft [43] and the examples, two orthogonal linearly polarized antennas with 90 degrees phase shift between their input ports can make a CP antenna. So the
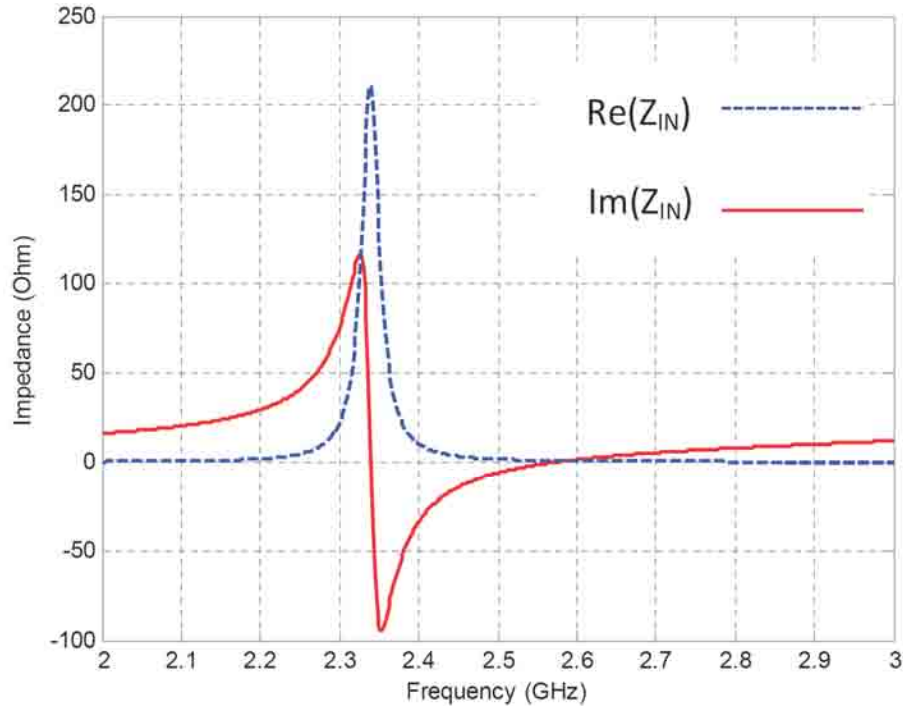
Fig. 3.3: Input impedance of a rectangular patch antenna.

square patch antenna can work as a CP antenna if we excite both ports with 90 degrees phase shift between port 1 and port 2. Right-Hand (RH) or Left-Land (LH) CP is defined based on +90 or −90 degrees phase difference between the ports.

The proposed square patch antenna with two ports is our final choice to support all polarizations. All harmonic suppression techniques reviewed before are good for antennas with one port, which means changing the geometry or adding shorting pins for one port will disturb the antenna behavior while excited with the other port. To find a solution it is good to have a look at input impedance of the antenna in different excitation modes and the surface current distribution at the fundamental frequency and the second harmonic.

The square patch antenna, shown in Fig. 3.5, was simulated in HFSS. It has dimensions of $L = W = 32.08\,mm$ on the RO4003C Rogers substrate. The relative permittivity was 3.55 and the thickness of the substrate was $32\,mil$ which is $h = 0.8128\,mm$. Excitation was with a lumped port and the input impedance of the patch was directly measured.

By simulating this patch with HFSS over a wide bandwidth to see input impedance
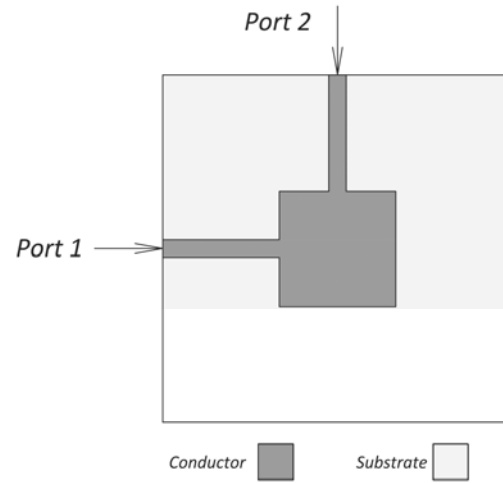
Fig. 3.4: LP and CP patch top view.
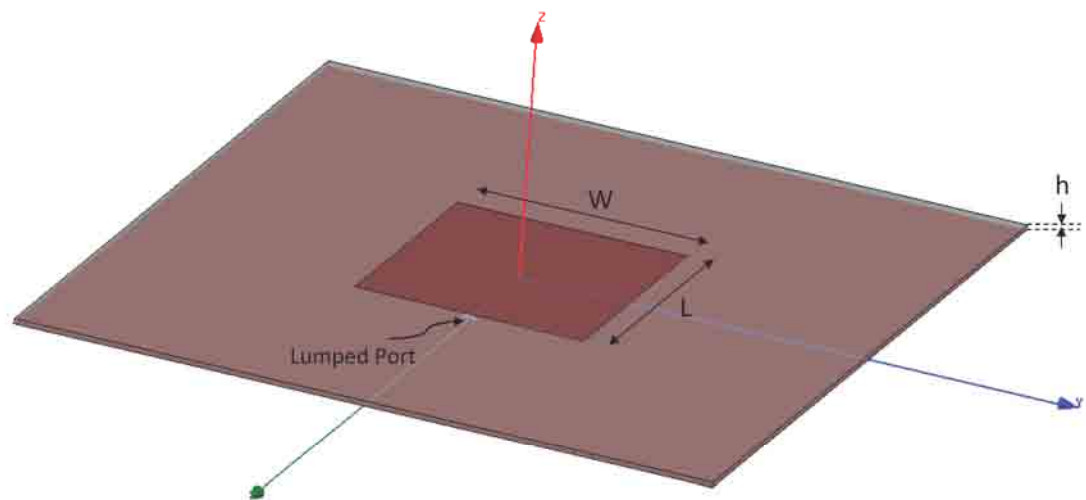
Fig. 3.5: Square patch antenna.

of a square patch antenna at the fundamental frequency and its harmonics, we can get the plot shown in Fig. 3.6. Each resonance happening around the frequencies where the real part of the input impedance is maximum and the imaginary part is zero. Six resonances are happening up to $9\,GHz$ and the frequency for each of them is written in Fig. 3.6.

Based on the design equations for the patch antenna, the fundamental frequency of operation for this antenna is at $f_1 = 2.374\,GHz$, as we can see in the Fig. 3.6, and the second and third harmonics are happening at $f_2 = 4.73\,GHz$ and $f_5 = 7.055\,GHz$. Other resonances are because of different modes current distributions on the patch which is not our interest. Current distribution for these three frequencies are shown in Fig. 3.7, Fig. 3.8, and Fig. 3.9. The maximum current is shown in red color and the minimum current is shown in blue.
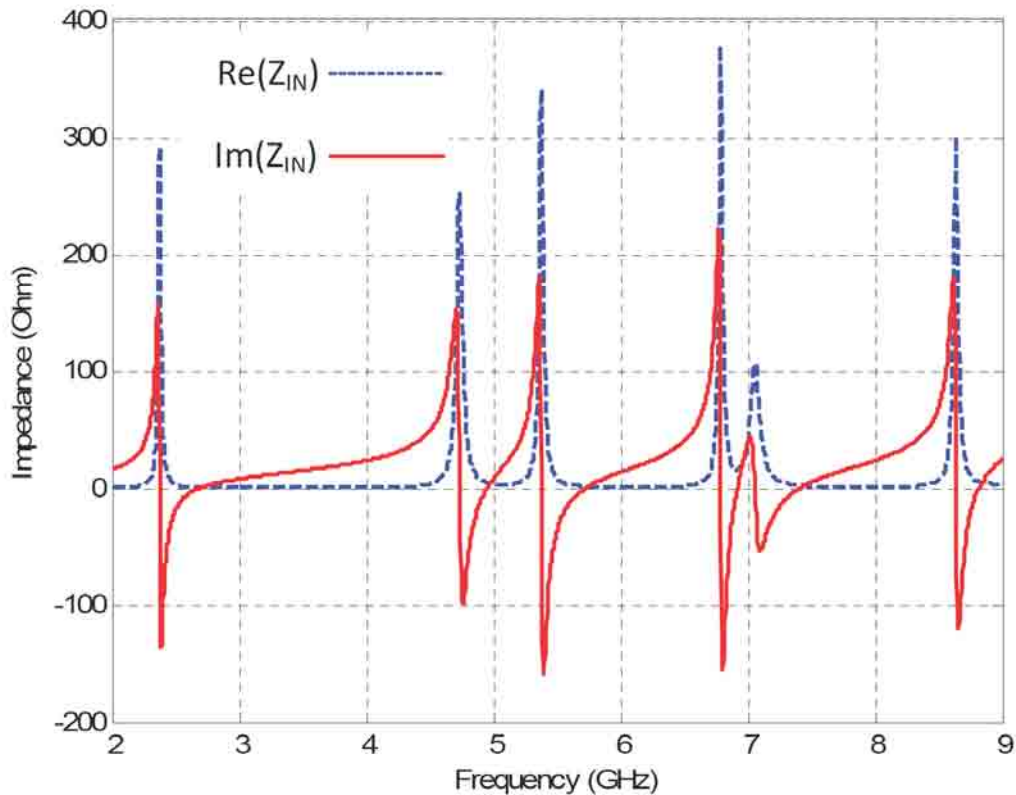
$f_1= 2.374\ GHz$ $f_2= 4.73\ GHz$ $f_3= 5.375\ GHz$ $f_4= 6.785\ GHz$ $f_5= 7.055\ GHz$ $f_6= 8.635\ GHz$

Fig. 3.6: Input impedance of the square patch antenna.

Fig. 3.7: Current distribution of the square patch antenna at the fundamental frequency of operation.

Fig. 3.8: Current distribution of the square patch antenna at its second harmonic.
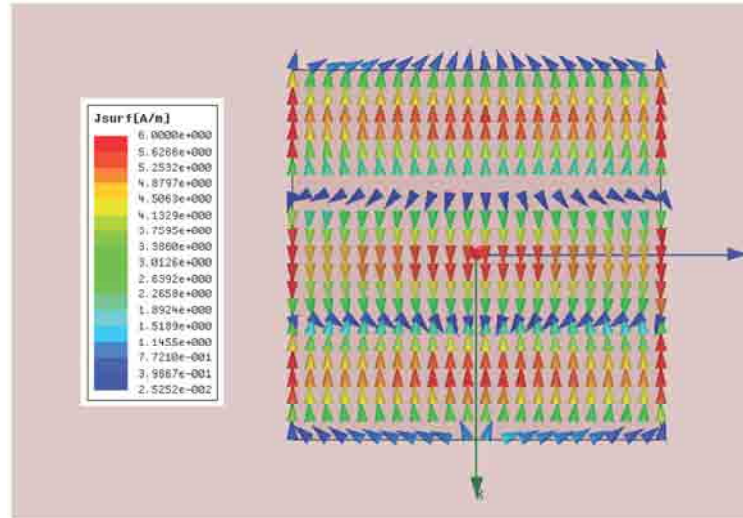
Fig. 3.9: Current distribution of the square patch antenna at its third harmonic.

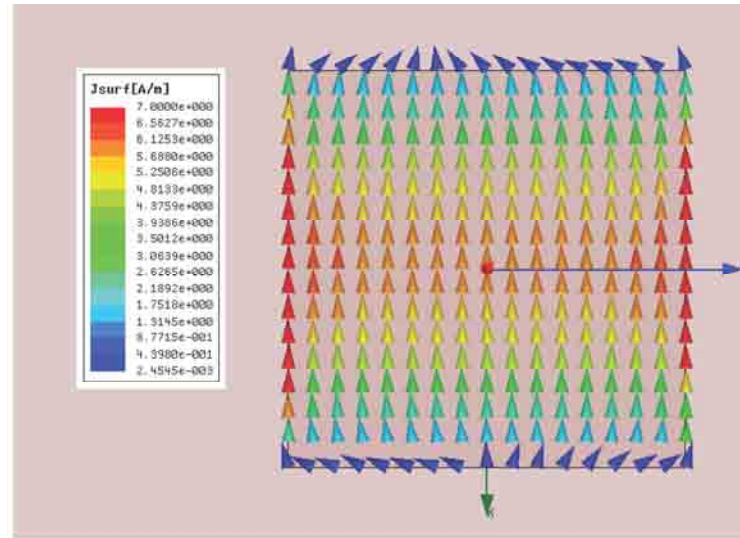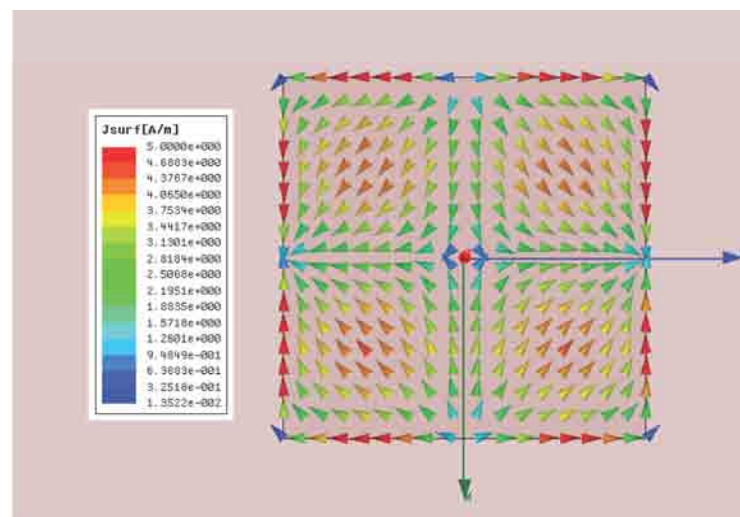Suppressing the second harmonic requires finding a method to change the current distribution in that mode while implying minimum change in current distribution of the fundamental mode. Dual port excitation for circular polarization has to be considered and that change should have the same effect on the antenna behavior for two orthogonal ports. The idea is to move the second harmonic response from its original frequency and increasing the current path for the second harmonic mode of the patch makes it possible. This could be done by introducing four slits on the patch as shown in Fig. 3.10. The surface currents of the second harmonic pass the longer path as illustrated and the resonance will happen at a lower frequency as a result.

These slits can move the second harmonic response to a lower frequency and as the final structure is symmetric, it would behave in the same way if there are two excitation ports for circular polarization. The slit's length and width should be optimized as well as the position of each on the patch. The longer the slit, the greater the frequency shift in the second harmonic. But we should take care of the fundamental behavior as we do not want to disturb the radiation pattern and linear polarization. The slit width cannot be more than a certain value because after that each of them will resonate as a slot antenna. The minimum for the slit width is dictated by the method of fabrication. For example, using a
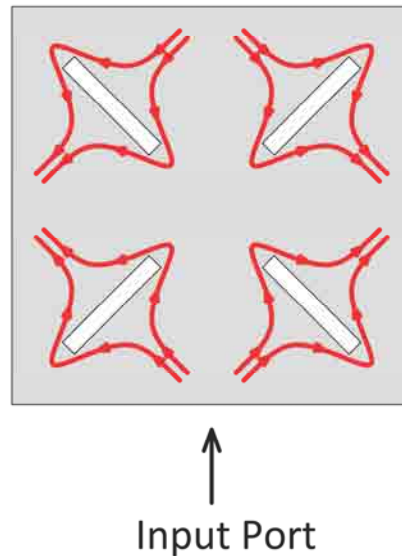
Fig. 3.10: Slits on a square patch to move the second harmonic response.

milling machine, it could not be less than $0.2\,mm$. Finally, for the position of the slits on the patch, they should not disturb antenna response at the fundamental frequency, as well as making maximum shift in the second harmonic response.

3.4 The Design of Square Patch Antenna with Harmonic Suppression

The proposed square patch antenna with harmonic suppressing slits was simulated. The antenna characteristics for linear and circular polarization are presented in the following two sections.

3.4.1 Linear Polarization

All simulations for the square patch antenna with the slits for harmonic suppressing are done with HFSS on the RO4003C substrate with $32\,mil$ thickness and the final optimum antenna is presented in Fig. 3.11. Introducing the slits will cause some frequency shift in the fundamental response of the patch and some change in the patch size is needed for the compensation. It has also higher input impedance as an additional effect of the slits on the

Fig. 3.11: Square patch antenna with harmonic suppression.

patch. The final dimensions of the harmonic suppressed antenna are: $L = W = 31\,mm$, $Slit\,Width = 0.25\,mm$, $Slit\,Length = 5.5\,mm$, and its distance from the corner of the patch is $d = 8.44\,mm$.

Simulation results for input impedance of the antenna are shown in Fig. 3.12 with all resonance frequencies. Although the fundamental frequency is $f_1 = 2.372\,GHz$ and i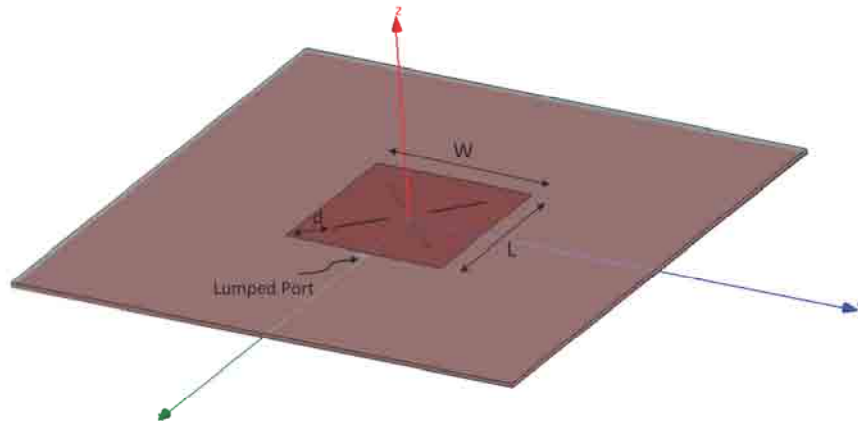ts second harmonic is expected to be about $4.7\,GHz$, the second resonance occurs at $f_2 = 4.4\,GHz$ which shows that the second harmonic is moved to $300\,MHz$ lower frequency.

In most of applications, the antenna is matched to a 50-ohm line, so the real 300-400 ohm input impedance should be transferred to 50 ohm using a quarter-wavelength transformer or by employing other methods for the matching circuit. In the AIA applications, however, the antenna input impedance could be any complex number and the matching network of the amplifier can accommodate it. In this case, the antenna can be used at another frequency near its resonance where the real part of input impedance is small but it has some imaginary part as well.

For example in Fig. 3.12, the antenna can be used at $f_1 = 2.4\,GHz$ where the input impedance is $Z_{IN} = 47.5 - j119.2 ohm$. This impedance can be used as the load for amplifier design instead of 50-ohm load. If we check the input impedance at the harmonics which are $f_2 = 4.8\,GHz$ and $f_3 = 7.2\,GHz$ they would be $0.8 + j\,10.7\,ohm$ at the second harmonic
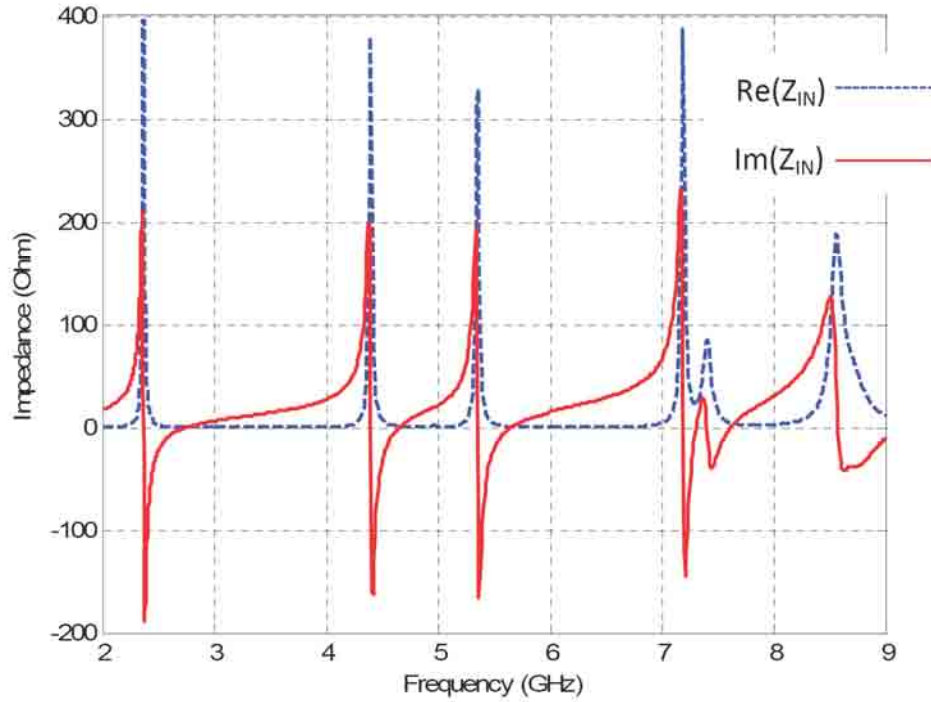
f_1= 2.372 GHz f_2= 4.4 GHz f_3= 5.36 GHz f_4= 7.19 GHz f_5= 7.40 GHz f_6= 8.56 GHz

Fig. 3.12: Input impedance of the square patch antenna with harmonic suppression.

and $295 - j\,119.4\,ohm$ at the third harmonic. The second harmonic is perfectly suppressed as the real part of input impedance is very close to zero and the third harmonic suppression is also acceptable as both real and imaginary parts are high impedances.

Normalized radiation patterns of this antenna are shown in Fig. 3.13 in two cuts of $\Phi = 0°$ and $\Phi = 90°$. The maximum directivity for this antenna is $7.47\,dB$ and for each plane both co-polar and cross-polar components are given. A strong co-polar component compared to cross-polar shows the linear polarization in this antenna.

3.4.2   Circular Polarization

For circular polarization, simulation for the same harmonic suppressed square patch antenna and two excitation ports can be done with HFSS. The schematic diagram for the antenna with two excitations is shown in Fig. 3.14. Both ports were excited with the same
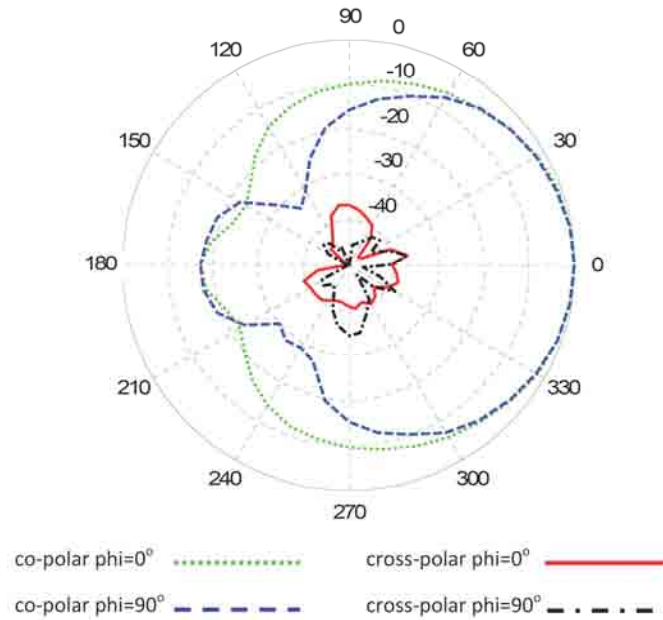
Fig. 3.13: Radiation pattern of LP square patch antenna with harmonic suppression at $2.4\,GHz$.

amplitude but a 90 degrees phase difference to maintain the circular polarization.

Normalized radiation patterns for this antenna are shown in Fig. 3.15 in two cuts of $\Phi = 0°$ and $\Phi = 90°$. For each plane both co-polar and cross-polar components for circular polarization are given. In a right-hand CP antenna, for example, the right-hand component is the co-polar and the left-hand component is the cross-polar for that antenna. A strong co-polar component compared with a cross-polar component in two planes means the antenna has perfectly circular polarization.

The best parameter to measure the circular polarization is Axial Ratio (AR). The plot for axial ratio around $2.4\,GHz$ is given in Fig. 3.16 and axial ratio of less than $3\,dB$ for circular polarization is observed.

The last thing to measure for an antenna with two ports is the isolation between the ports. Leakage from one port to the other one is not accepted. This could be measured by S_{21}, which is the transferred signal to port 2 when port 1 is excited. The result is shown in Fig. 3.17 and better than $25\,dB$ isolation is achieved.

As a conclusion, the square patch antenna with harmonic suppressing slits can still
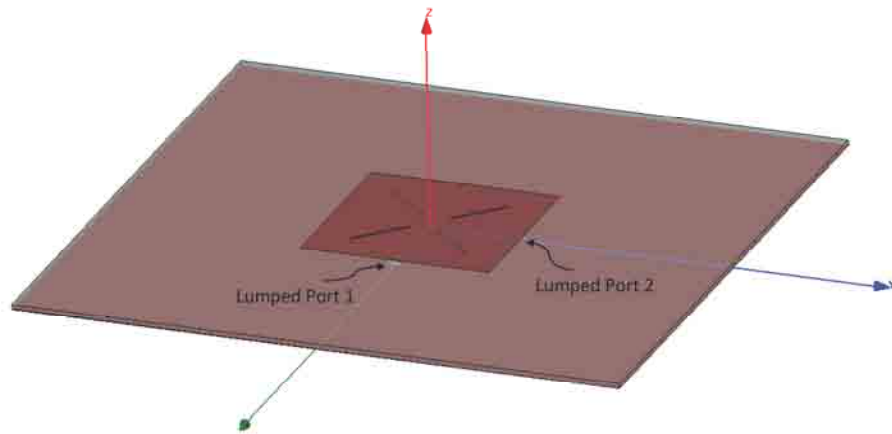
Fig. 3.14: The CP square patch antenna with harmonic suppression.
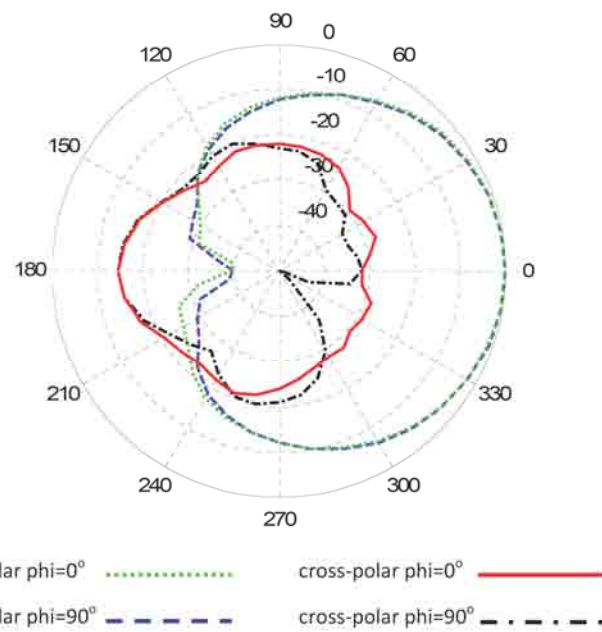
Fig. 3.15: Radiation pattern of CP square patch antenna with harmonic suppression.
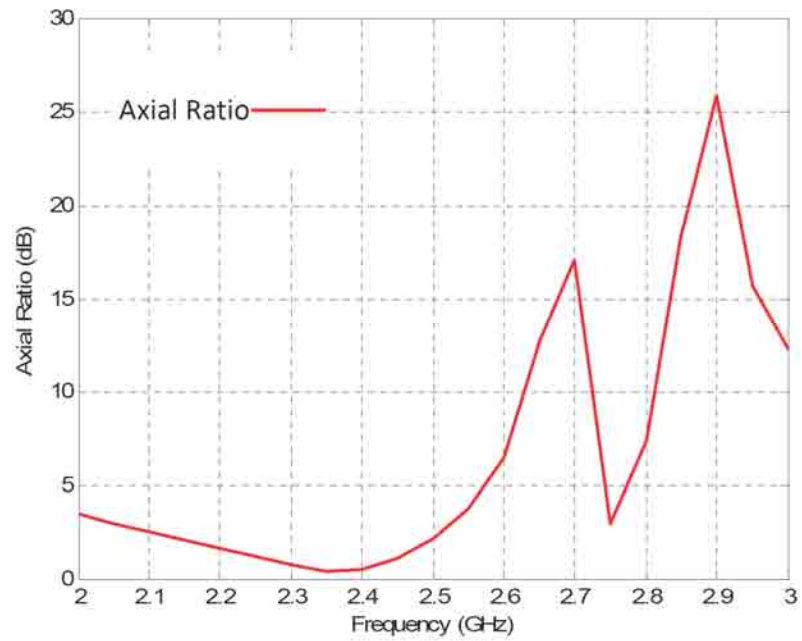
Fig. 3.16: Axial ratio of the CP square patch antenna with harmonic suppression.
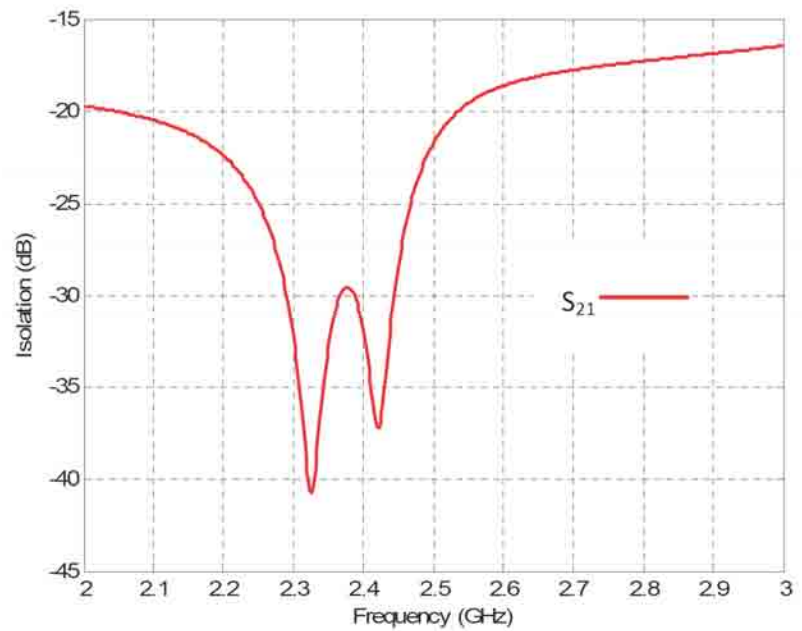
Fig. 3.17: Isolation between two ports of CP square patch antenna with harmonic suppression.

work as a linearly polarized antenna. It means the patch can be used with two ports for circular polarization and the result of simulation perfectly agrees with it. In the next two chapters, this antenna is used as a load of the amplifier for linear and circular polarization applications and the results of measurement are provided.

Chapter 4

Linearly Polarized Active Integrated Antenna

4.1   Prototype of the Active Integrated Antenna

For an active LP antenna, the designed patch antenna should be directly connected to the amplifier's output as its load. Input impedance of the antenna can be used as a frequency dependent load in ADS simulation. All steps of amplifier simulation would be the same as the instruction in Chapter 2.

Two amplifiers were designed for two patch antennas. The first one is matched to the simple square patch and the second one is matched to the square patch with harmonic suppression. So PAE for two circuits can be compared and the improvement caused by harmonic suppression were calculated in this way. Two antennas shown in Fig. 3.5 and Fig. 3.11 are used as the load and their input impedances are considered in amplifier design procedure. Both amplifiers are designed with ADS on the $32\,mil$ RO4003C substrate using the same transistor, NESG2031M16, and optimized for maximum performance for a class B amplifier at $2.4\,GHz$. The layout of the amplifier integrated with the simple patch is shown in Fig. 4.1 and the AutoCAD layout of the amplifier integrated with the patch antenna with harmonic suppression is shown in Fig. 4.2 with all lumped element values the same as the amplifier in Chapter 2.

Patch antenna and amplifier circuit are fabricated on the same substrate using a milling machine. Other steps of soldering are as explained in Chapter 2. Each circuit has only one SMA connector for the input port and the output is the antenna which radiates to free space. Both fabricated antennas with their amplifiers are shown in Fig. 4.3 and Fig. 4.4. The method of measurement and the results are provided in the next sections.
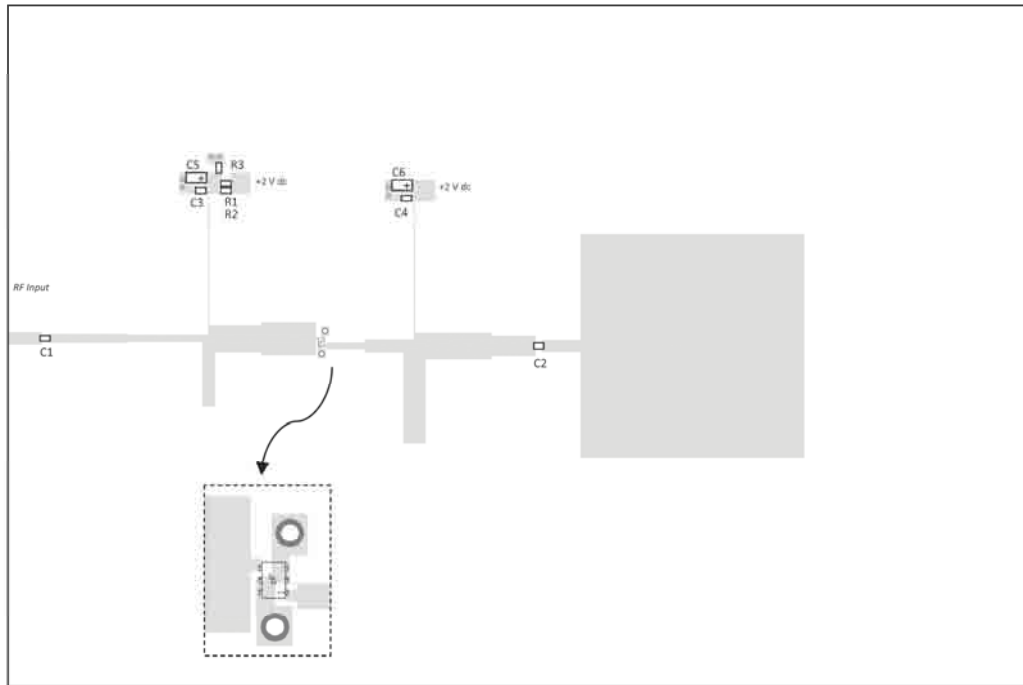
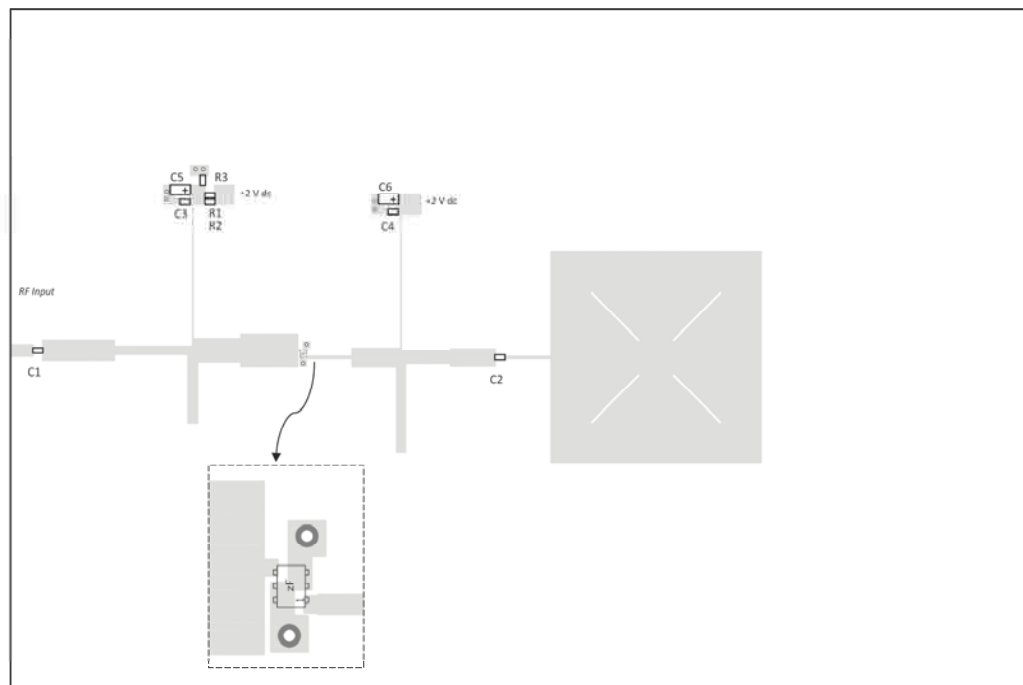Fig. 4.1: Layout of $2.4\,GHz$ amplifier integrated with square patch antenna.

Fig. 4.2: Layout of $2.4\,GHz$ amplifier integrated with square patch antenna with harmonic suppression.
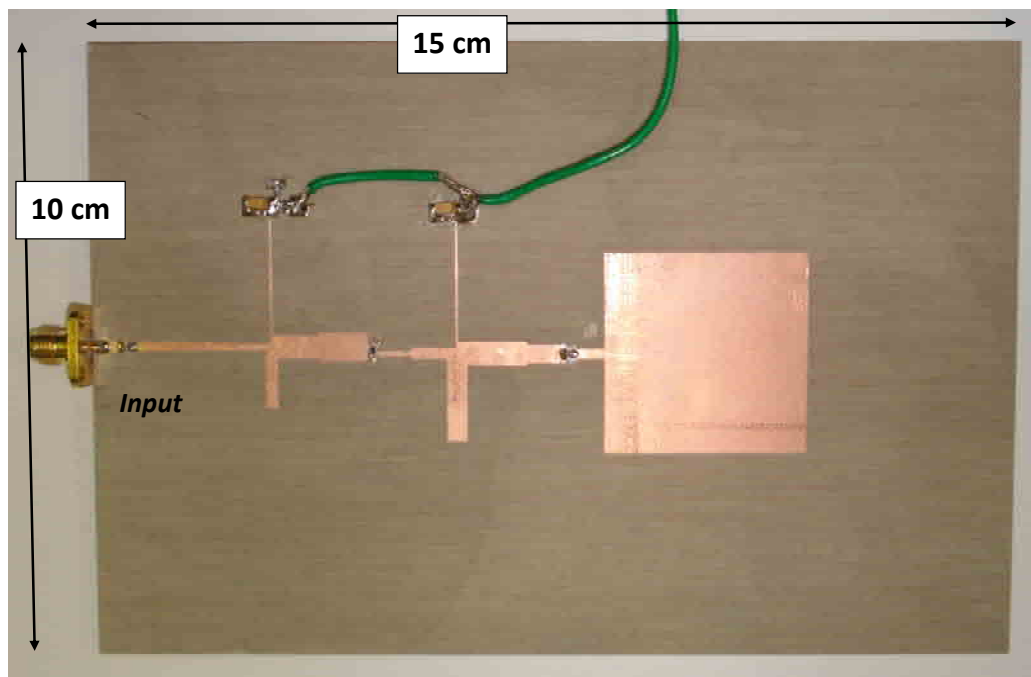
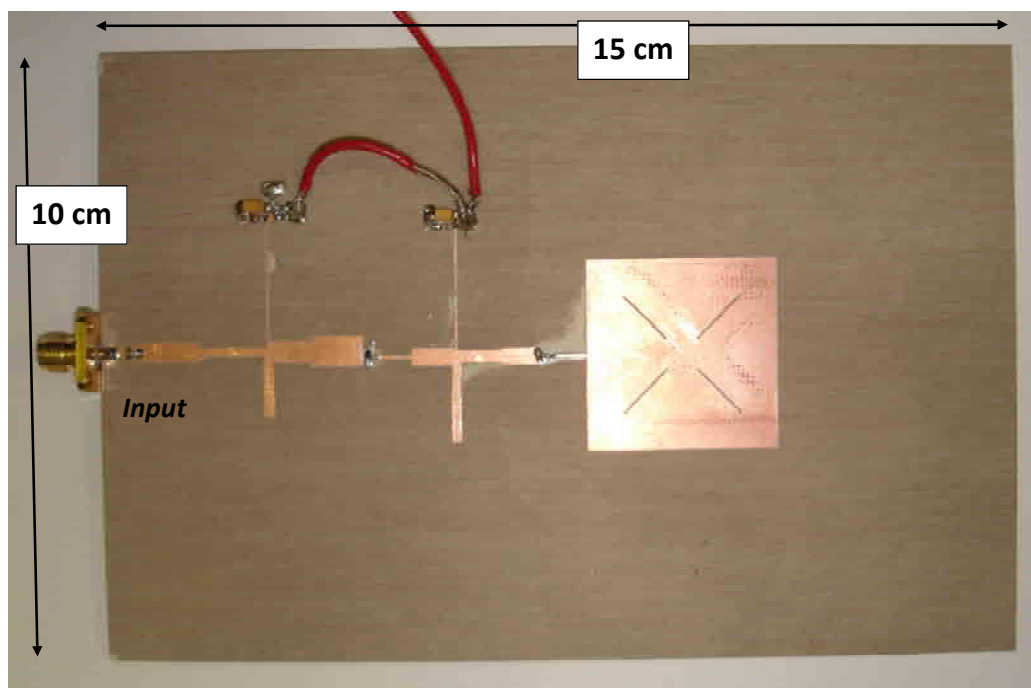Fig. 4.3: Fabricated 2.4 GHz amplifier integrated with square patch antenna.

Fig. 4.4: Fabricated 2.4 GHz amplifier integrated with square patch antenna with harmonic suppression.

4.2   Output Power and PAE Measurement Method

The amplifier's output power is normally measured using a power meter or spectrum analyzer. All these instruments are usually 50 ohm for RF systems and the amplifier's output port is assumed to be 50 ohm as well. In our design, as the antenna has arbitrary input impedance and the amplifier is conjugate matched to it, we cannot fabricate the amplifier without antenna and measure the output power. The antenna should be connected to the amplifier anyway to provide maximum power delivery. Other tools like a high impedance probe or active probe can be used to measure the output power of the amplifier while it is connected to the antenna. This method is not accurate for power measurement and it is just acceptable for comparing the power level of the signal in different parts of the circuit. In AIA, introducing the probe close to the patch is also disturbing antenna behavior and causing a change in its input impedance which can affect the amplifier's performance.

One reliable method is doing the measurement inside an anechoic chamber using the Friis transmission equation [6–8, 10]. This equation (4.1) in free space is expressing the relation between power level of received signal P_r and transmitted signal P_t with the transmit antenna gain G_T, the receive antenna gain G_r, the wavelength of signal λ, the reflection coefficients in the transmitter Γ_t and the receiver Γ_r, the polarization vector of the transmit antenna $\mathbf{a}_t$ and the receive antenna $\mathbf{a}_r$, the absorption coefficient of the intervening medium α, and the distance R between two antennas.

$$\frac{P_r}{P_t} = G_t \, G_r \, \left(1 - |\Gamma_t|^2\right) \, \left(1 - |\Gamma_r|^2\right) \, |\mathbf{a}_t \cdot \mathbf{a}_r^*|^2 \, e^{-\alpha R} \left(\frac{\lambda}{4\pi R}\right)^2 \tag{4.1}$$

One antenna is the receiver which is the near-field probe shown in Fig. 4.5 and the transmit antenna is the Antenna Under Test (AUT) and its gain is known from HFSS simulation. AUT is connected to the RF signal source and the receiver to the spectrum analyzer for power measurement. These two antennas should be aligned inside the chamber pointing at each other and with zero degrees angle between their polarization vectors. These two alignments could be verified by moving or rotating one antenna around its position to find the situation with maximum received power.
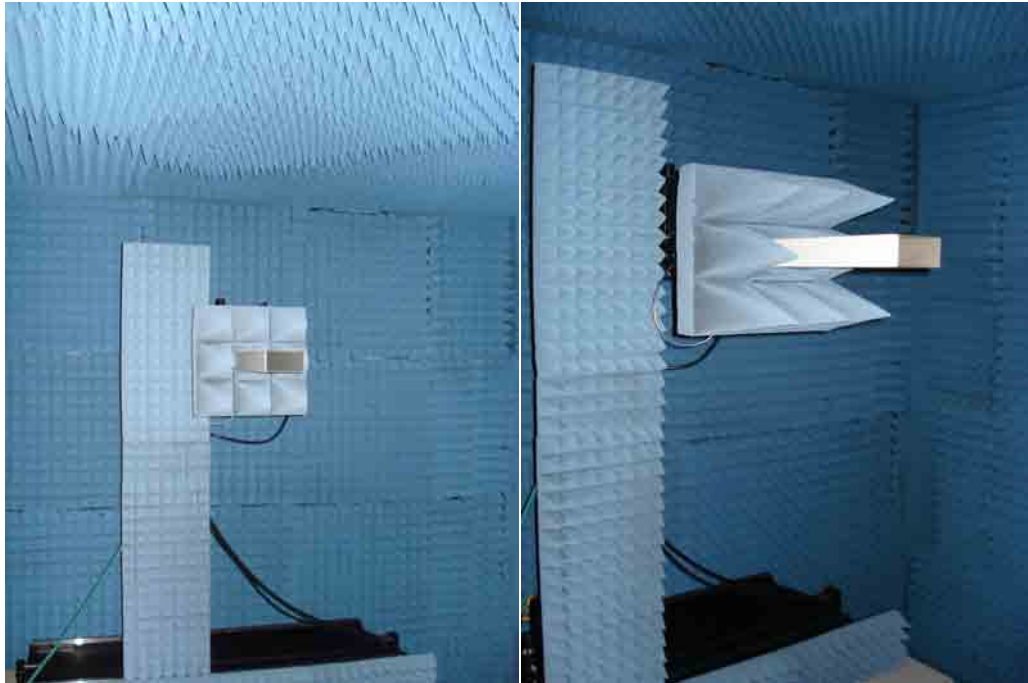
Fig. 4.5: Near-field probe as the receive antenna.

There are three losses inherent in the measurement: cable loss from the signal source to the AUT, free space path loss between two antennas, and the cable loss from the receiver to the spectrum analyzer. As we are interested to measure the amplifier and antenna behavior, other parameters like the distance, frequency, and loss of connecting cables should be considered fixed during different measurements. It is also important to consider the matching of the antennas and the effect of absorption coefficient of the intervening medium not changing in different measurements.

4.2.1   Calibrating the Measurement Setup

As explained in the previous section, all the parameters in the Friis transmission equation, except the transmit power and the transmit antenna gain, have to be fixed, so the received power found to depend on the transmit power. The rest of the parameters can be considered to be constant in the measurement by calibrating the measurement setup. The equation (4.1) was modified to equation (4.2) where all the loss in the system and the receive antenna gain is put in one part as L and the performance is presented in dB.

$$P_r \ (dBm) = P_t \ (dBm) + G_t \ (dB) + L \ (dB) \qquad (4.2)$$

This calibration can be done by using a patch antenna as AUT, shown in Fig. 4.6, with known gain which is fed with an arbitrary input power like $0 \ dBm$. By measuring the received power and using equation (4.2), L in dB could be found which is going to be as a fixed value in the next measurements.

This simple patch antenna is a square patch shown in Fig. 4.7. As the input impedance of this patch is high we used coupling method to match it to a 50-ohm line. The dimensions are $L = W = 32.6 \ mm$, $L_T = 23 \ mm$, $W_T = 0.3 \ mm$, $g = 0.2 \ mm$, and $W_{Line} = 1.8 \ mm$. Antenna gain is $6.029 \ dB$ at its resonance frequency from the simulation and the plot of S_{11} for the measurement is given in Fig. 4.8.
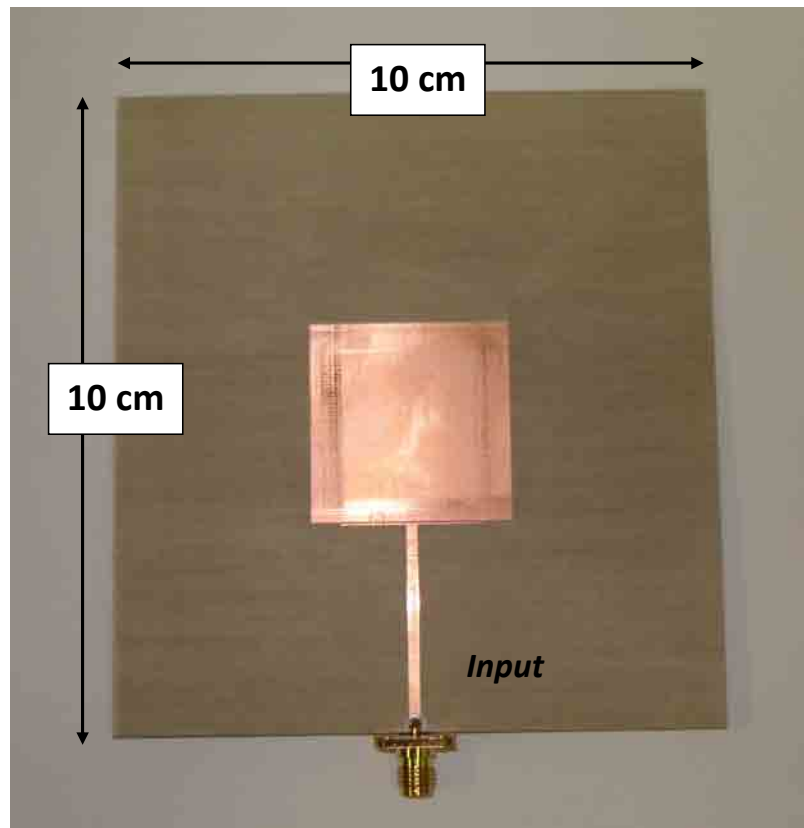

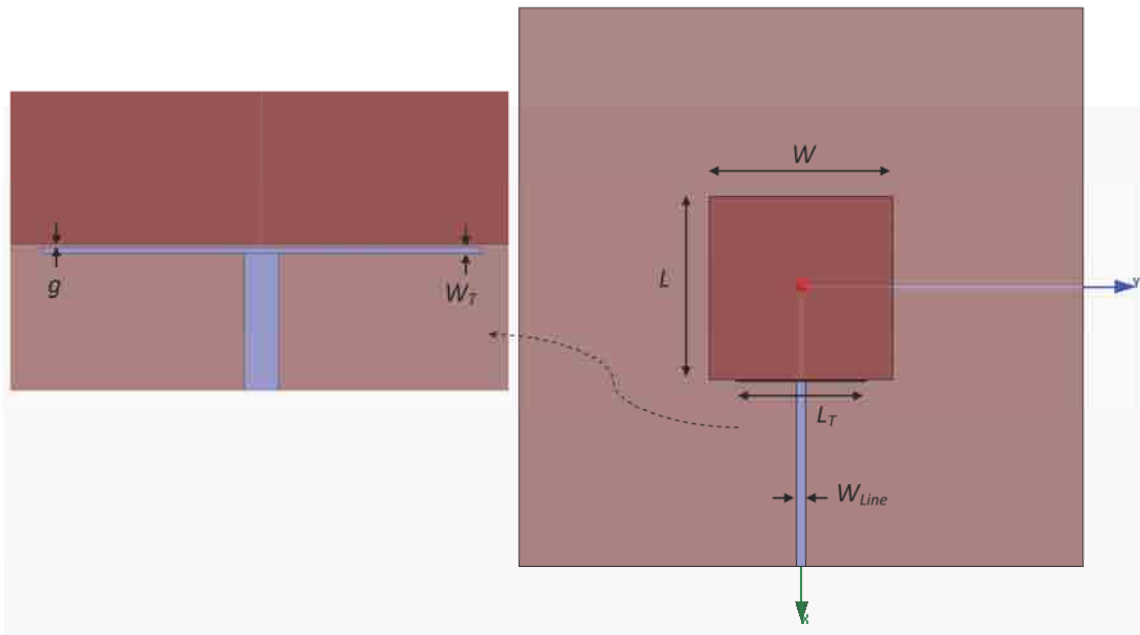Fig. 4.6: Simple patch used for calibration.

Fig. 4.7: Simple patch antenna with coupling port's schematic and dimensions.
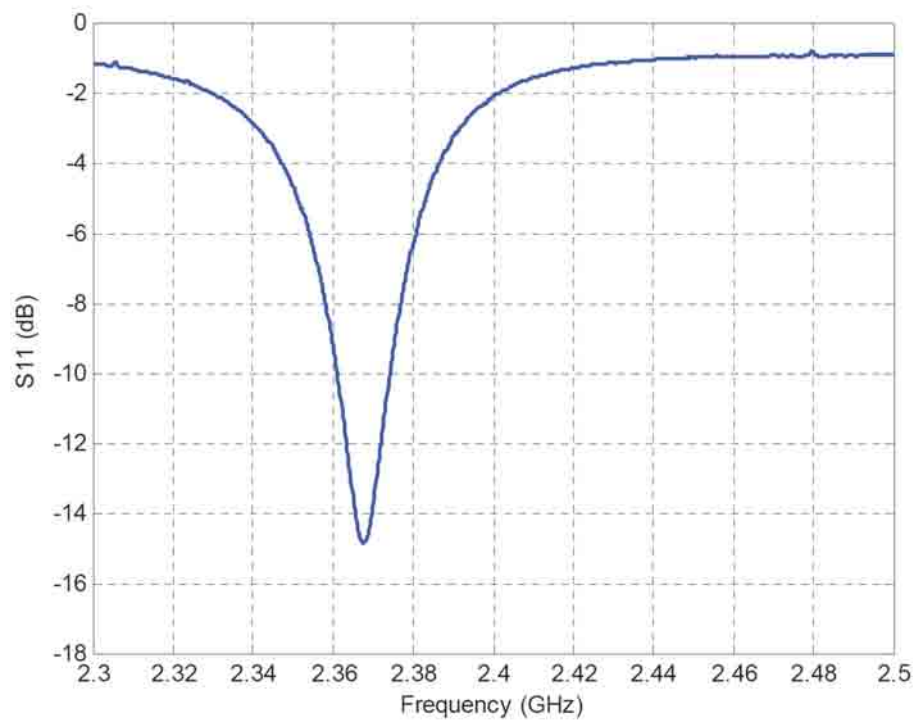

Fig. 4.8: Measurement results of S_{11} for the simple patch antenna with coupling port.

4.2.2   Measurement of 2.4 GHz Amplifier Integrated with the Square Patch Antenna

Using the same measurement setup and by placing the active antenna at the transmitter side we can measure the received power using a spectrum analyzer. The received power would be more than the measurement in the previous section due to the use of an amplifier and some possible differences in two antenna gains. Using equation (4.2) and considering the square patch antenna gain from the simulation $6.226\,dB$ and $L = -45.129\,dB$ from the calibration measurement, the amplifier's gain G_A is found using equation (4.3).

$$P_r\ (dBm) = P_t\ (dBm) + G_A\ (dB) + G_t\ (dB) + L\ (dB) \tag{4.3}$$

Output power P_{OUT} of the amplifier using equation (4.4) is needed to calculate PAE. Input power P_{IN} is calculated from equation (4.5) where the signal source power level P_{SOURCE} and all input cables loss $Cable\ Loss$ are known.

$$P_{OUT}\ (dBm) = P_{IN}\ (dBm) + G_A\ (dB) \tag{4.4}$$

$$P_{IN}\ (dBm) = P_{SOURCE}\ (dBm) - Cable\ Loss\ (dB) \tag{4.5}$$

By changing the signal source power level and measuring the received power level, the plot for amplifier's output power versus the amplifier input power at a fixed frequency is obtained. DC power consumption for each input power level is measured using a volt meter and ampere meter at the same time. Measurement setup is shown in Fig. 4.9 and the results are given in the next section.

4.3   Results and Discussions

Two amplifier simulations have been performed using ADS. The first simulation is for the amplifier which is matched to the simple patch antenna. The antenna input impedance is used as the load characteristic in the simulation. The second simulation is for the amplifier which is matched to the patch antenna with harmonic suppression. The design for each
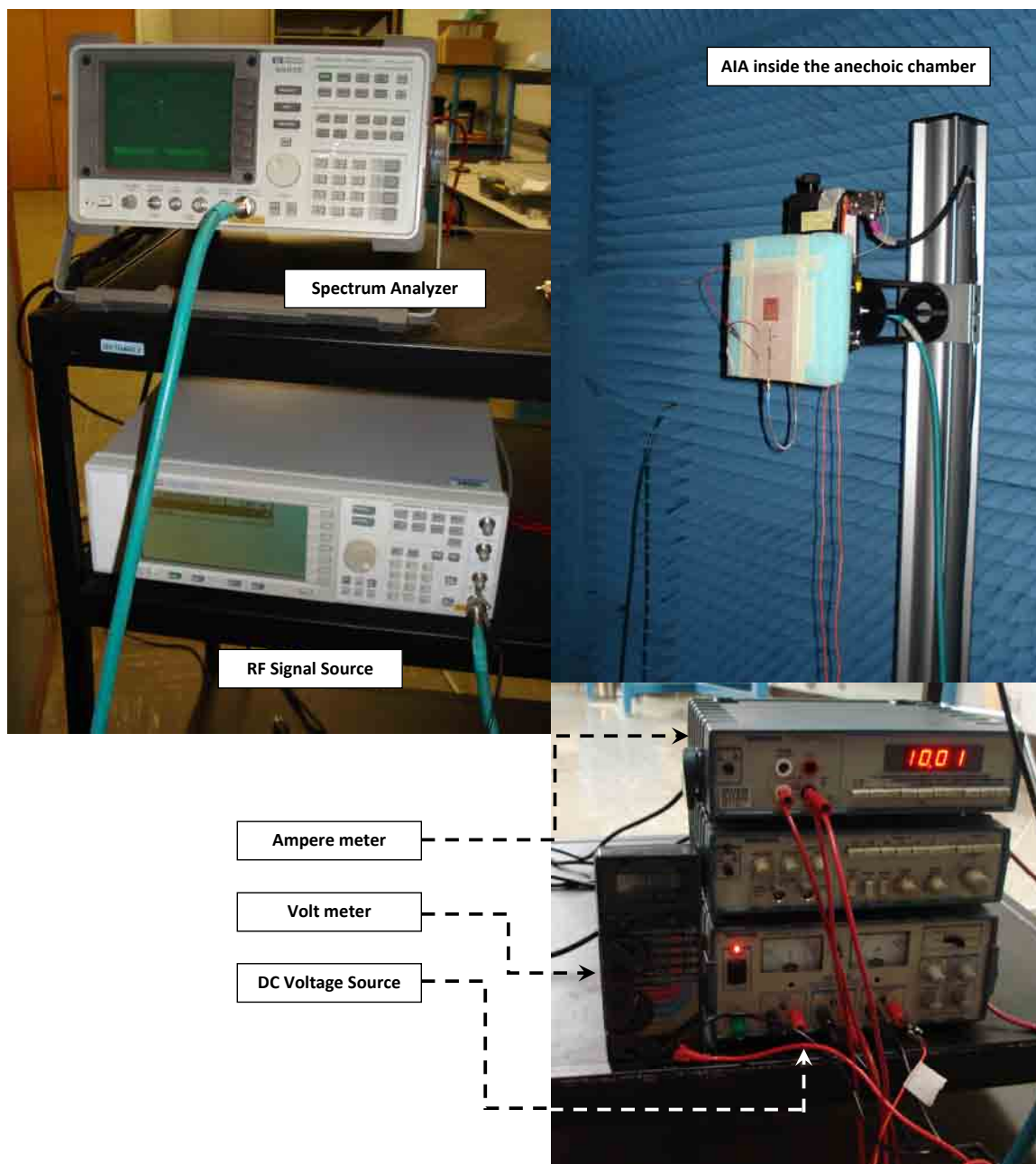
Fig. 4.9: Measurement setup for power measurement.

amplifier is based on the impedance of the antenna at its resonance frequency. As there is some difference between the impedance of two antennas at their fundamental frequency, the matching circuits for two amplifiers are different as a result. If we want to compare the performance of two antennas based on harmonic suppression, it is meaningful if the rest of the circuits for both antennas are the same. In our experiment we have two different circuits and if we want to compare, we should just consider the difference in PAE in two circuits even if they have different output power curves.

The results of amplifier simulations are shown in Fig. 4.10 and Fig. 4.11. The first figure compares output power and the second compares PAE for the amplifiers integrated with two antennas with and without harmonic suppression. It is clear that there is 4.5% improvement in PAE when the antenna with harmonic suppression is used as the load of the amplifier compared with the simple antenna behavior. All simulation results are at $2.4\,GHz$ as the antenna and amplifier center frequency.
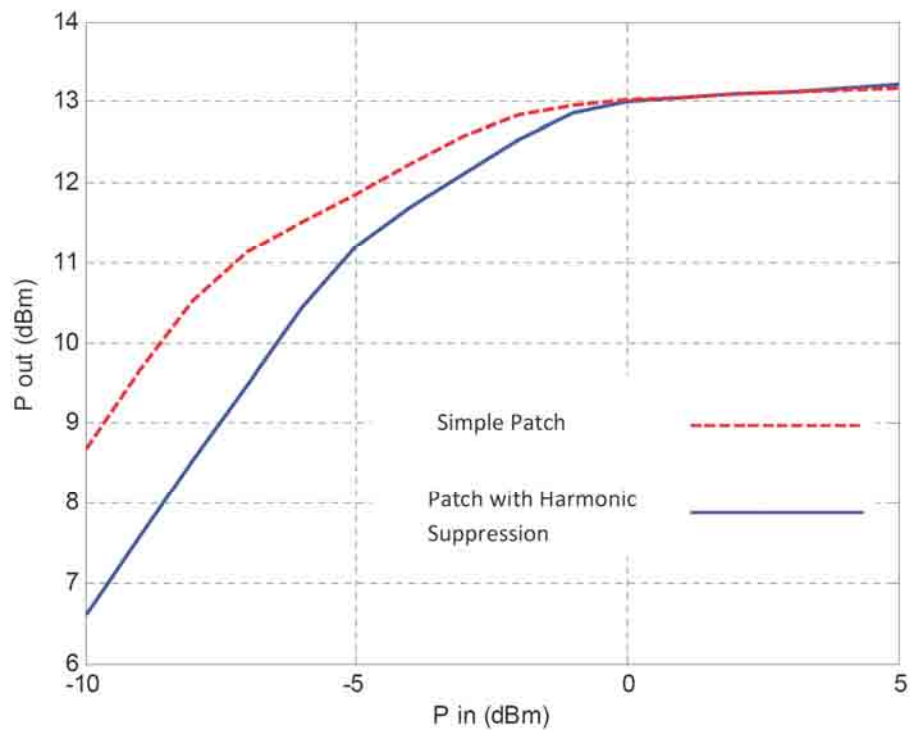

Fig. 4.10: Simulation results of output power for simple patch and the patch with harmonic suppression.
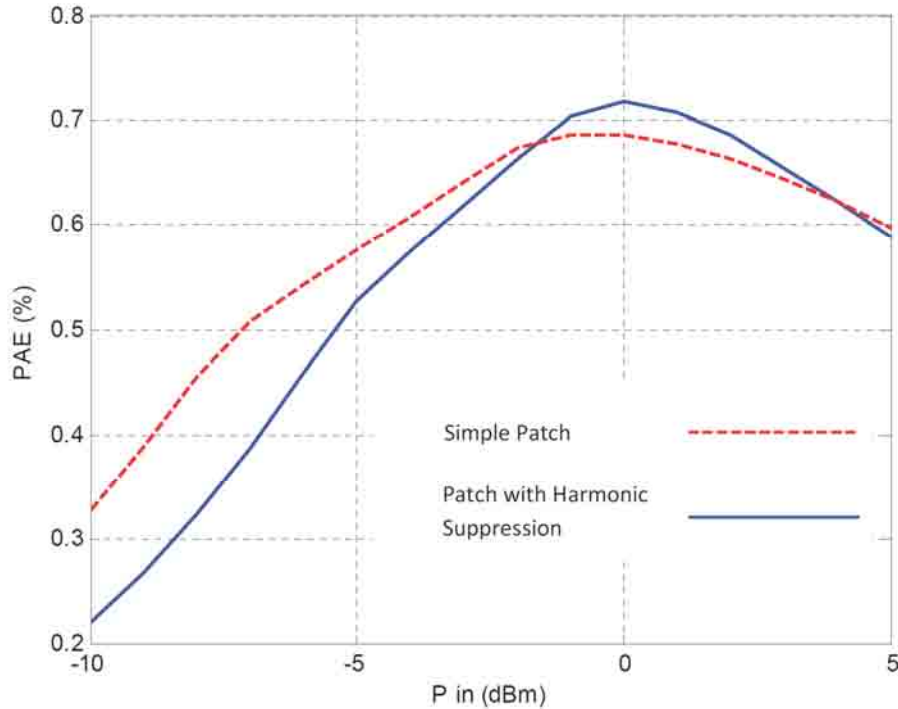
Fig. 4.11: Simulation results of PAE for simple patch and the patch with harmonic suppression.

By conducting the measurement method as described in the previous section, the results of output power and PAE measurement for two antennas are given in Fig. 4.12 and Fig. 4.13. About $0.3\,dB$ improvement was observed in the output power for the amplifier matched to the antenna with harmonic suppression compared with the simple patch. This improvement is due to the harmonic suppression as the output power is concentrating in the fundamental frequency and the difference in matching circuits of two amplifiers. However, as a result we can see $4-5\%$ improvement in PAE, which is very close to the simulation results.

All above measurements were performed at a single frequency for each antenna. Frequency of $2.415\,GHz$ was selected as the frequency of measurement for the simple patch and $2.4\,GHz$ for the patch with harmonic suppression. These frequencies were chosen based on S_{11} measurement for both active antennas. The plots for these measurements are given in Fig. 4.14. Both AIAs have almost the same bandwidth but we were able to improve PAE by harmonic suppression in the antenna.

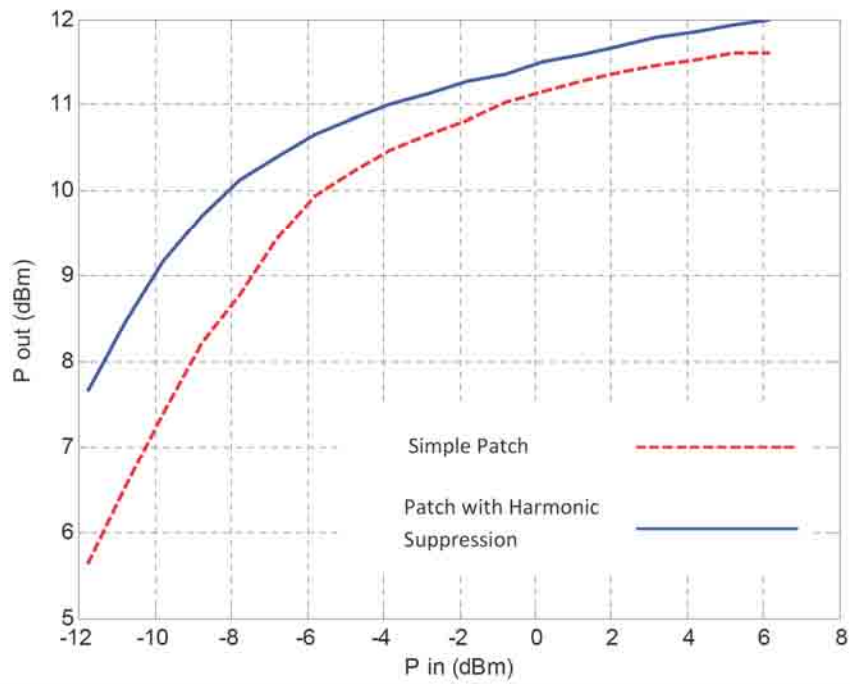Fig. 4.12: Measurement results of output power for simple patch and the patch with harmonic suppression.
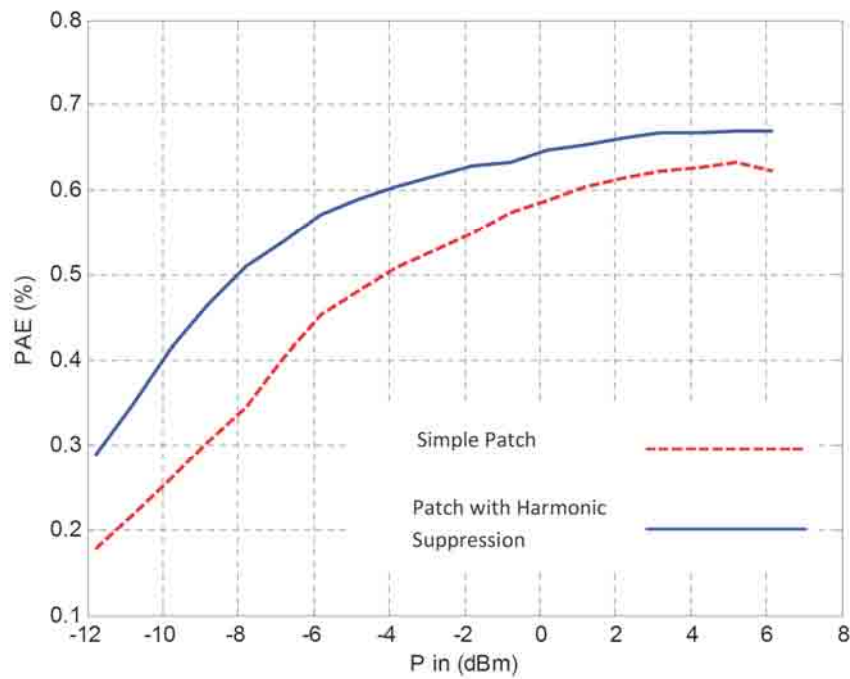

Fig. 4.13: Measurement results of PAE for simple patch and the patch with harmonic suppression.
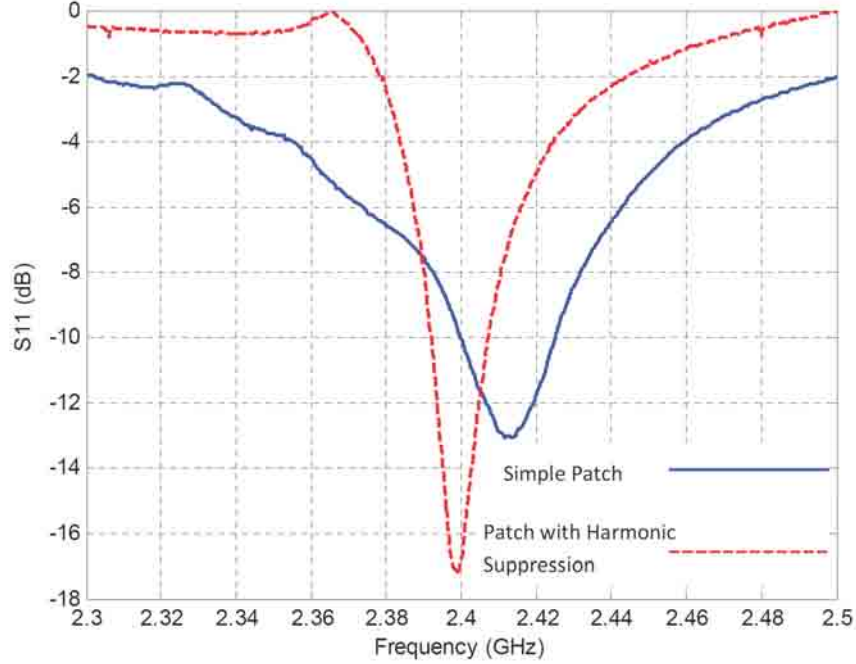
Fig. 4.14: S_{11} plots for simple patch and the patch with harmonic suppression both integrated with the amplifier.

After considering the amplifier behavior in two circuits, we measured the radiation pattern of each antenna. This measurement was conducted using the NSI near-field measurement equipments [45] inside the anechoic chamber. For each antenna the radiation pattern could be measured in two planes of $\Phi = 0°$ and $\Phi = 90°$. For the simple patch antenna at $2.415\,GHz$, the radiation pattern of the $\Phi = 0°$ cut is shown in Fig. 4.15 and for $\Phi = 90°$ is shown in Fig. 4.16. For each plane both co-polar and cross-polar components are given for comparison from both the simulation and the measurement. The maximum directivity for the simple patch after the measurement is $7.15\,dB$ while it is $7.63\,dB$ in the simulation.

The same measurement for the patch antenna with harmonic suppression was performed at $2.4\,GHz$ and the results are given in Fig. 4.17 and Fig. 4.18. The maximum directivity for the patch with harmonic suppression after the measurement is $6.91\,dB$ while it is $7.47\,dB$ in the simulation.

In the measurement results of radiation pattern for both antennas we can see good

Fig. 4.15: Radiation pattern of simple patch antenna at 2.415 GHz integrated with the amplifier in $\Phi = 0°$ cut.

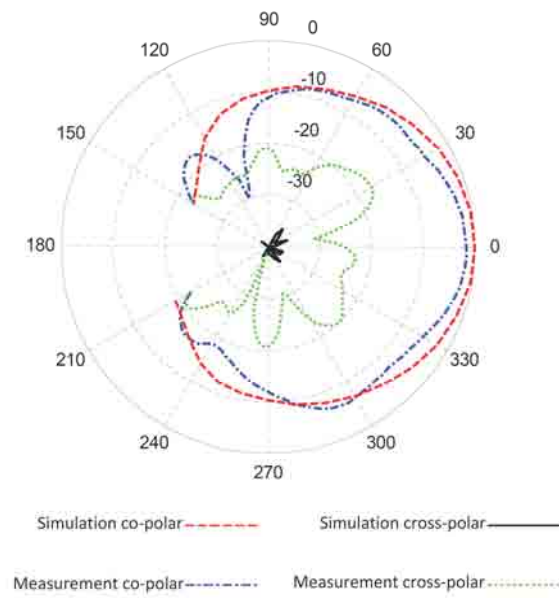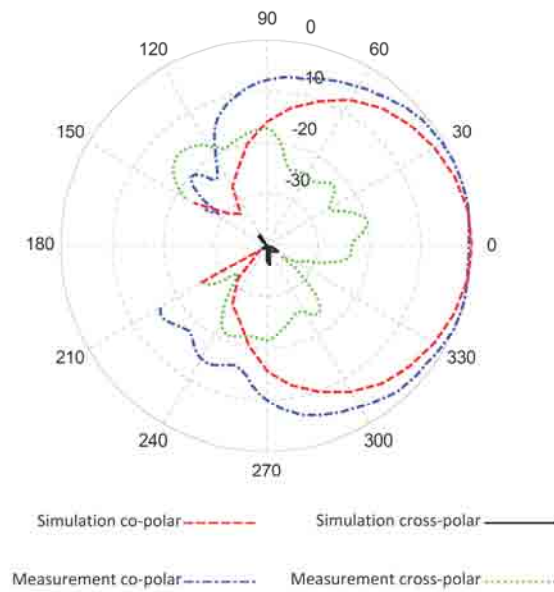Fig. 4.16: Radiation pattern of simple patch antenna at 2.415 GHz integrated with the amplifier in $\Phi = 90°$ cut.
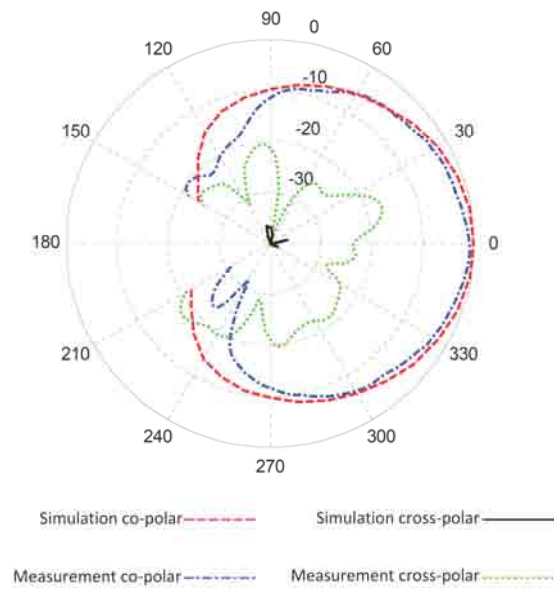
Fig. 4.17: Radiation pattern of the patch antenna with harmonic suppression at $2.4\,GHz$ integrated with the amplifier in $\Phi = 0°$ cut.
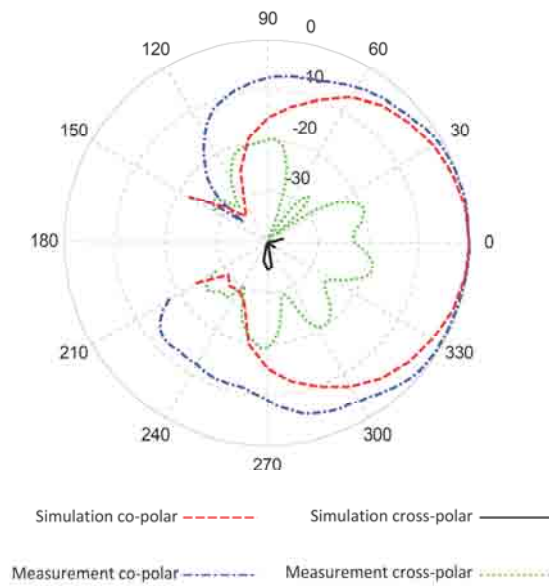
Fig. 4.18: Radiation pattern of the patch antenna with harmonic suppression at $2.4\,GHz$ integrated with the amplifier $\Phi = 90°$ cut.

agreement between co-polar components. Although cross-polar components are still 20 dB lower than co-polar components at the direction of maximum directivity which shows good linearity in polarization, the cross-polar components are much stronger than the simulation. This is because of the radiation effect of the amplifier circuit which is attached to the antenna. In all HFSS simulations for the antenna we just considered the square patch directly excited with a lumped port but in reality, the structure is not that simple and all parts of amplifier circuit can disturb radiation behavior of the antenna. These parts should have the same effect on the co-polar components, but the co-polar component is strong enough and the impact is negligible. As described in Chapter 3, this LP patch antenna with symmetric structure is a good element to be used for circular polarization applications just by 90 degrees phase shift between two excitation ports. The circular structure and measurement process is expressed in the next chapter.

Chapter 5

Circularly Polarized Active Integrated Antenna

5.1 Design Considerations

As explained in Chapter 3, the proposed CP antenna is one square LP antenna with two orthogonal excitation ports with 90 degrees phase difference between them. The active CP antenna has two amplifier circuits connected to the edges of the antenna. As the antenna is the same from Chapter 4 with known input impedance, amplifier circuits are duplicates from active LP antenna. The last step to achieve circular polarization is equal power level excitation with 90 degrees phase difference. The phase difference can be provided using an external component or by implementing it inside the circuit. This component is introduced in the next section.

5.2 The 3-dB Hybrid

Branch-line coupler is a 3-dB power divider which provides 90 degrees phase difference between its outputs. Microwave passive devices with these properties all generally called Quadrature Hybrids. The design equations are explained in Pozar [16], so we can perform the design in a microstrip structure on our substrate and integrate it with the amplifier circuit to provide input signals for each amplifier with the same magnitude and the appropriate phase difference. The approach divides the input RF signal into two signals with equal power levels which means $3\,dB$ less power level in the output ports. In practice there is more than $3\,dB$ drop in each port due to transmission loss and mismatch at the ports of the coupler.

Design steps were performed at $2.4\,GHz$ on the same substrate and ADS layout simulation results using Method of Momentum (MOM) are found. The AutoCAD layout is given

in Fig. 5.1 showing four ports all are 50-ohm microstrip transmission line on the specified substrate.

If we excite from port 1 we expect to see about $-3\,dB$ for S_{21} and S_{31}, good isolation at port 4 which means $S_{41} < -20\,dB$, and good matching for all four ports $S_{11}, S_{22}, S_{33}, S_{44} < -20\,dB$. As the structure is symmetric, measurement of one port's matching like S_{11} is sufficient. Simulation results for magnitude of S-parameters are given in Fig. 5.2.

The other important characteristic for this branch-line coupler is the phase difference between two output ports, i.e. ports 2 and 3. Looking at phase of S_{21} and S_{31} in simulation, they show the phase of each output port considering the same reference port which is port 1. The difference between those values would be the phase difference between the output ports of this coupler. The simulation results for the phase of S_{21} and S_{31} are given in Fig. 5.3. Difference of 90 degrees between two phases shows the appropriate phase difference between two output ports.
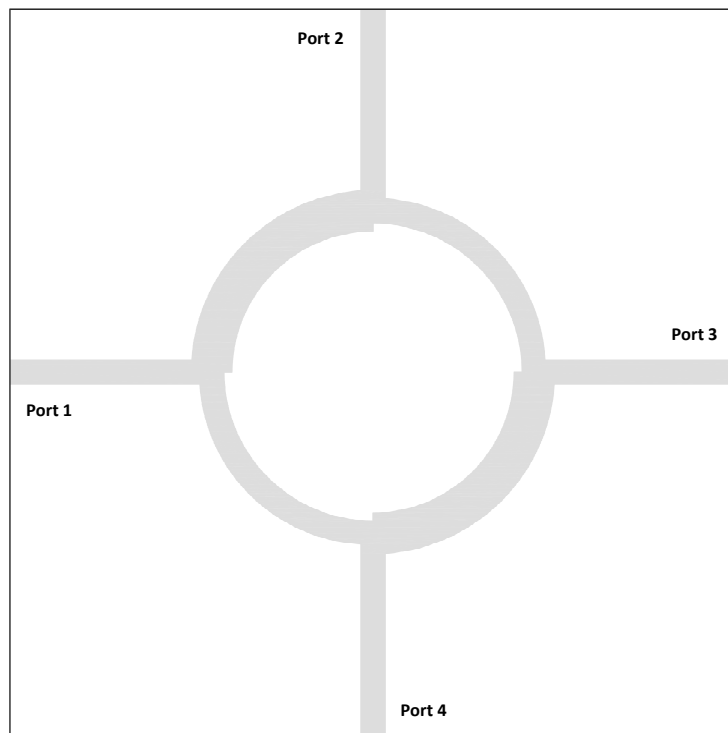

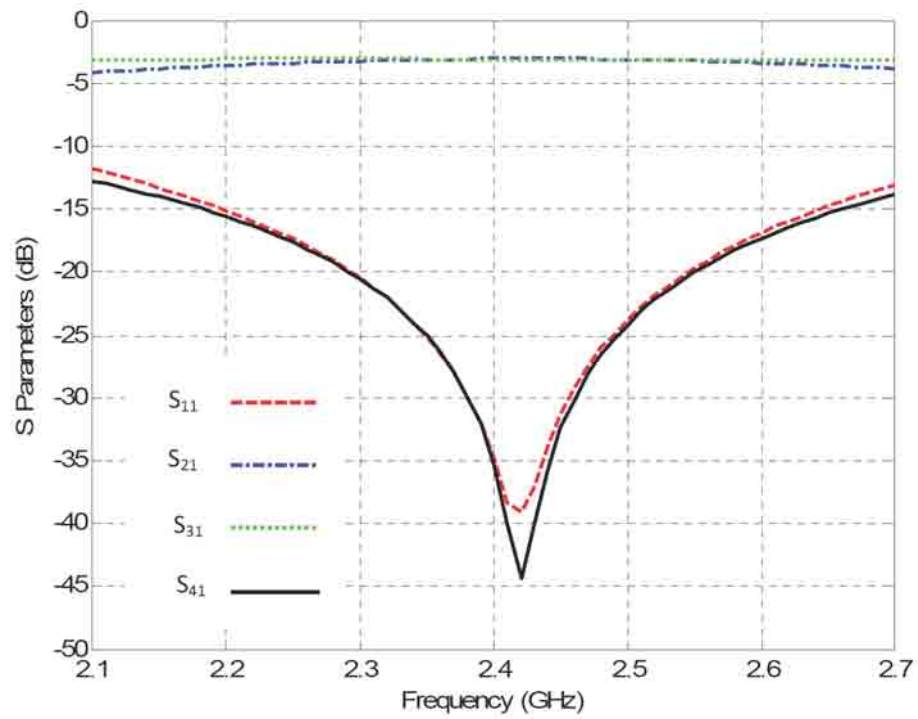Fig. 5.1: Layout of branch-line coupler at $2.4\,GHz$.

Fig. 5.2: Simulation results for magnitude of S-parameters for the branch-line coupler.
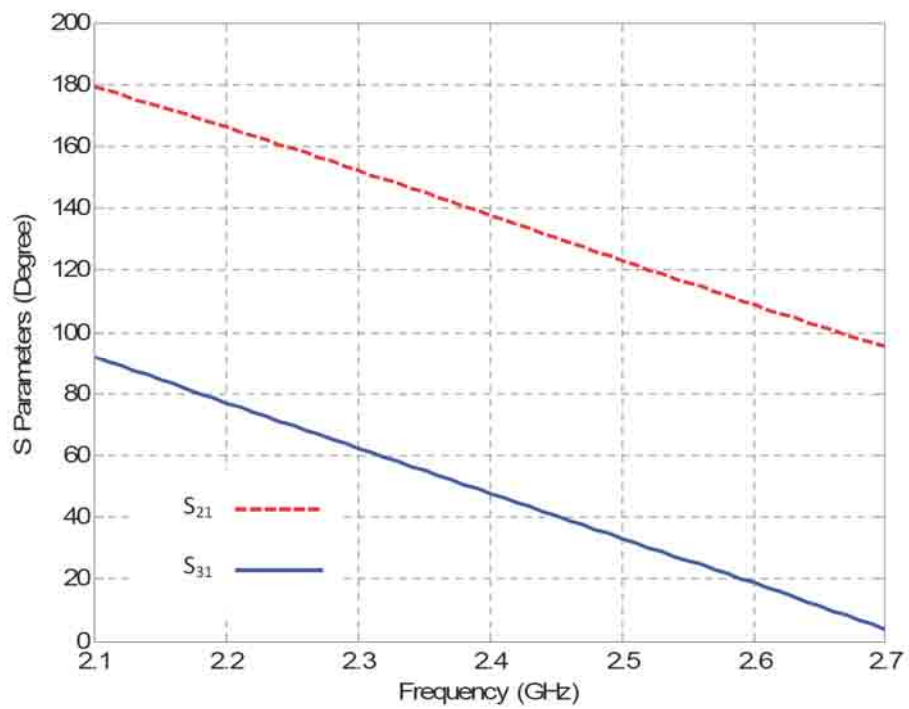

Fig. 5.3: Simulation results for phase of S_{21} and S_{31} for the branch-line coupler.

The coupler is fabricated on the same RO4003C substrate using a milling machine and the measurement was done using Agilent 8510C Vector Network Analyzer (VNA). As this VNA has two ports for measurement, two other ports of the coupler have to be matched using 50-ohm loads. The fabricated branch-line coupler and two steps of measurement are shown in Fig. 5.4.

The measurement results for magnitude of S-parameters are given in Fig. 5.5. As the structure is symmetric we just conducted the test for S_{11} and expected to have almost the same matching results for other ports. We are just interested to see the equal power division between ports 2 and 3, therefore only the magnitude of S_{21} and S_{31} are being measured.

Measurement results for the phase of S_{21} and S_{31} are given in Fig. 5.6 and 90 degrees phase difference between two output ports is observed.

Considering measurement results for the branch-line coupler, this hybrid is suitable to provide input RF signal for the amplifier circuits with the same magnitude and 90 degrees phase shift. In this way we can have circular polarization for the patch antenna with harmonic suppression.
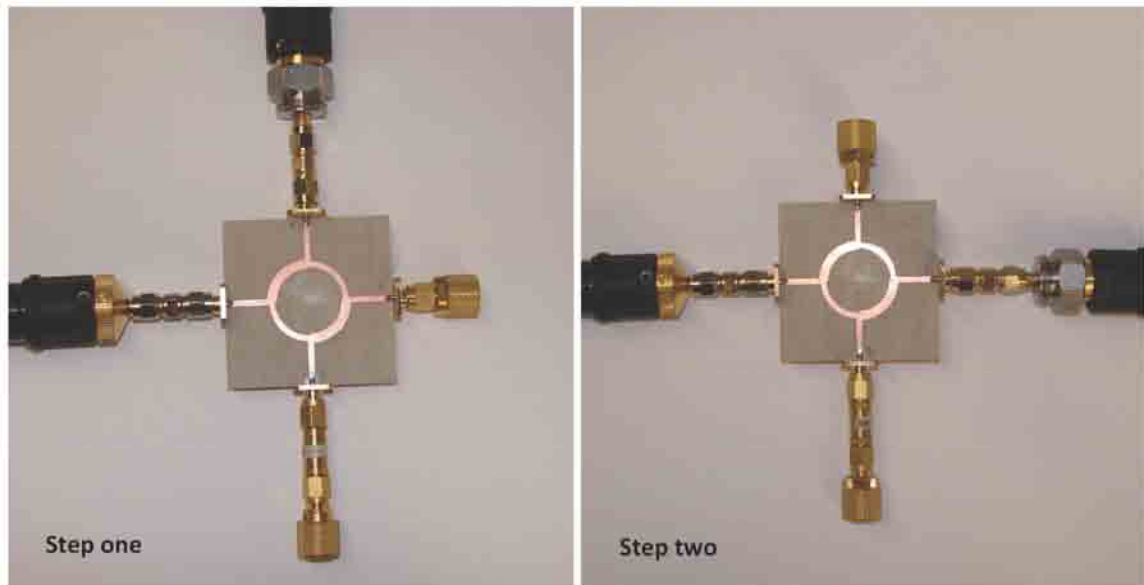
Fig. 5.4: The fabricated branch-line coupler and measurement steps.
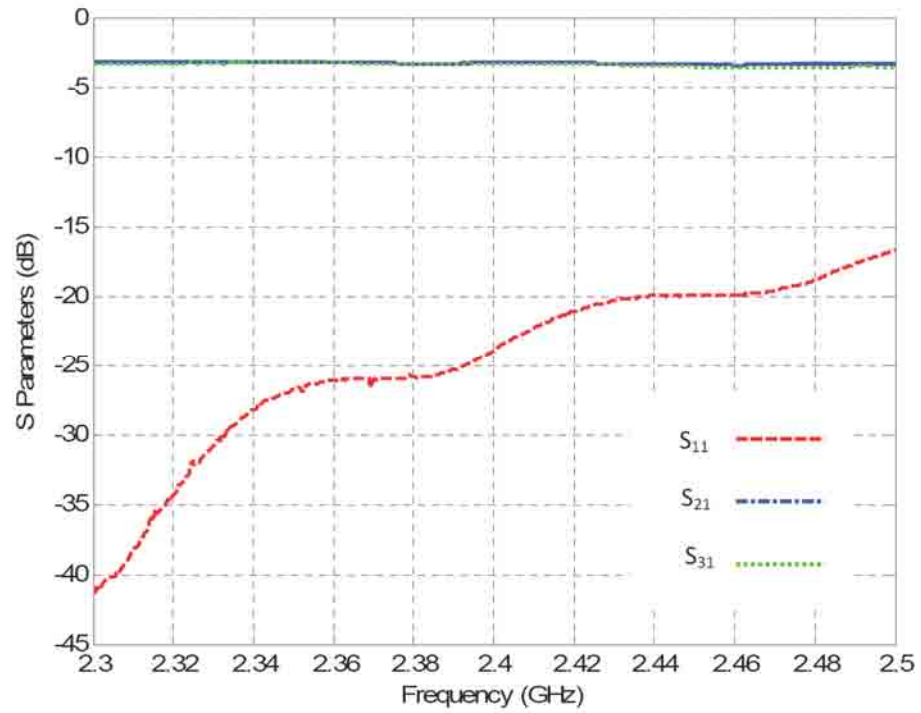
Fig. 5.5: Measurement results for magnitude of S-parameters for the branch-line coupler.
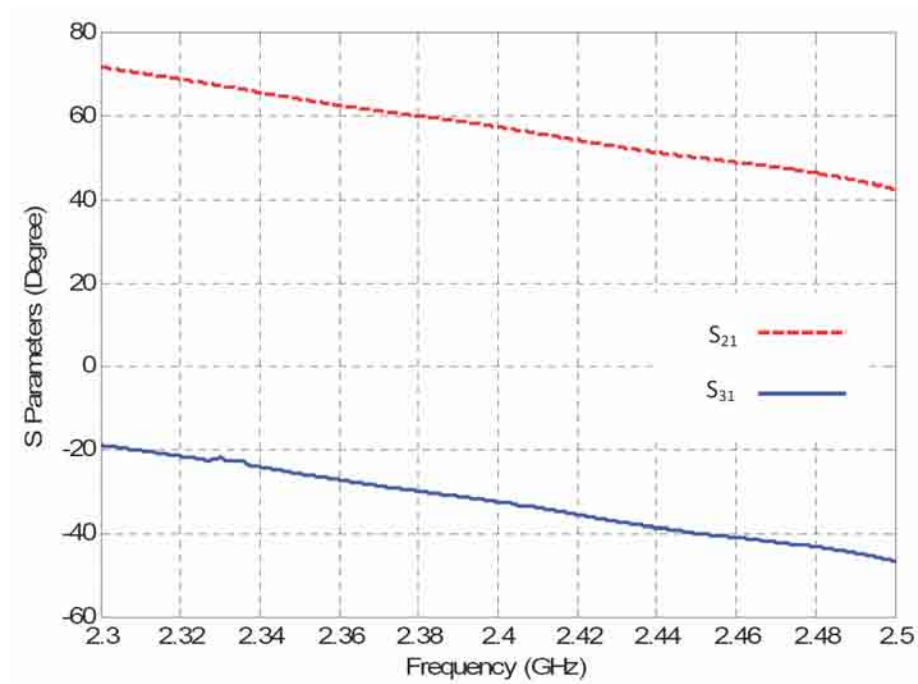
Fig. 5.6: Measurement results for phase of S_{21} and S_{31} for the branch-line coupler.

5.3 Fabrication of Active Integrated CP Antenna and Measurement Results

All needed components to achieve an active integrated CP antenna with harmonic suppression are designed and the last step is to draw the final layout using the square patch with harmonic suppression, two amplifier layouts, and the branch-line coupler. The AutoCAD layout is given in Fig. 5.7 showing the antenna and two amplifiers circuits with the lumped elements having the same values as described in Chapter 2.
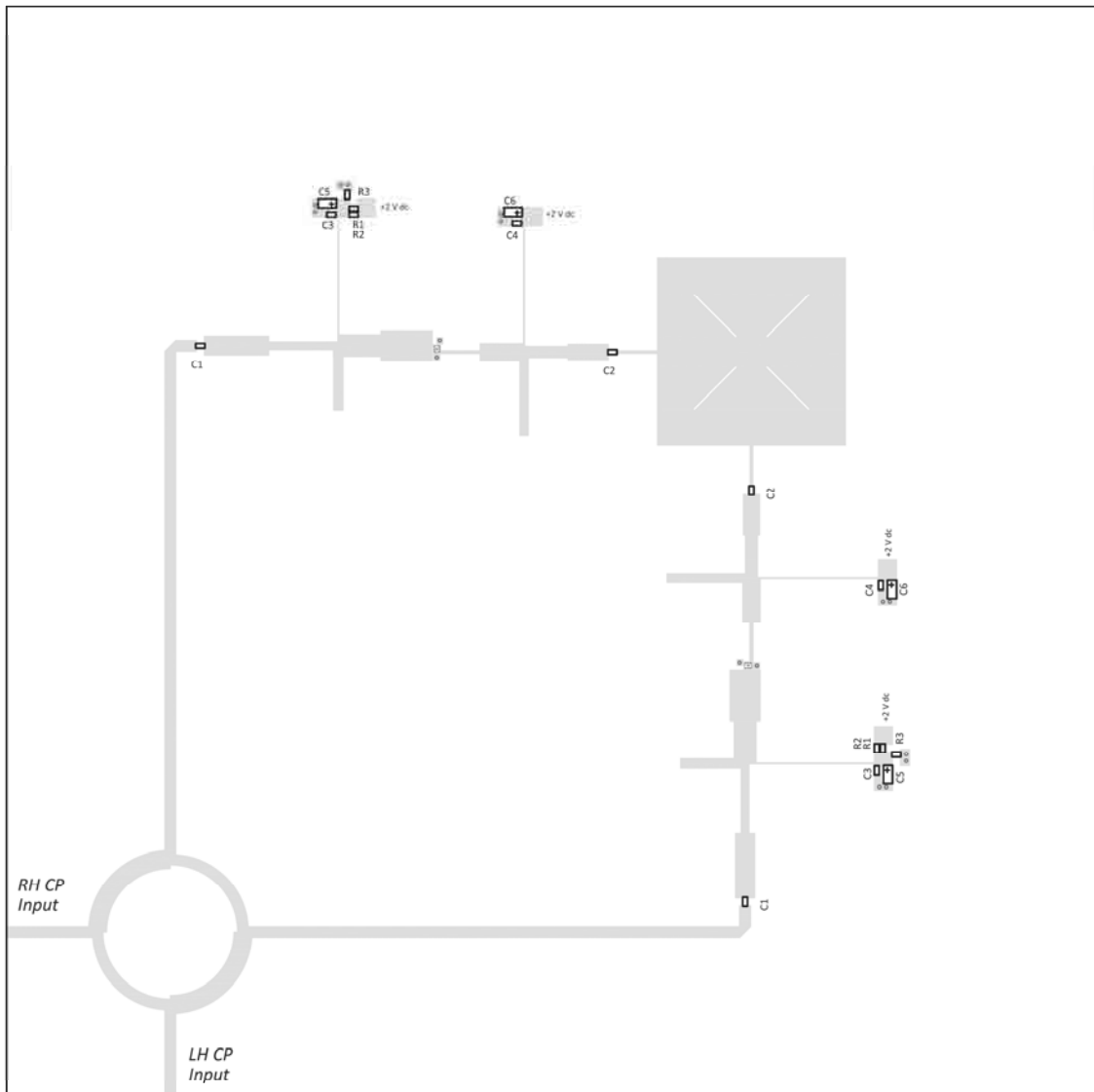
Fig. 5.7: Layout of CP active integrated antenna with harmonic suppression at $2.4\,GHz$.

The complete circuit was fabricated on the RO4003C substrate as shown in Fig. 5.8. Two SMA ports are shown in the figure. One is used as the input port and the other should be matched to 50-ohm load as the isolated port. Using either of them as an input port for excitation is possible and the difference is in right-hand or left-hand circular polarization for the antenna.

Fig. 5.8: Fabricated CP active integrated antenna with harmonic suppression at $2.4\,GHz$.

For this antenna to measure the circular polarization we used NSI near field range inside the anechoic chamber. The active antenna was placed as the transmitter and the near field probe used as the receiver and two co-polar and cross-polar components for the circular polarization were measured. For example in th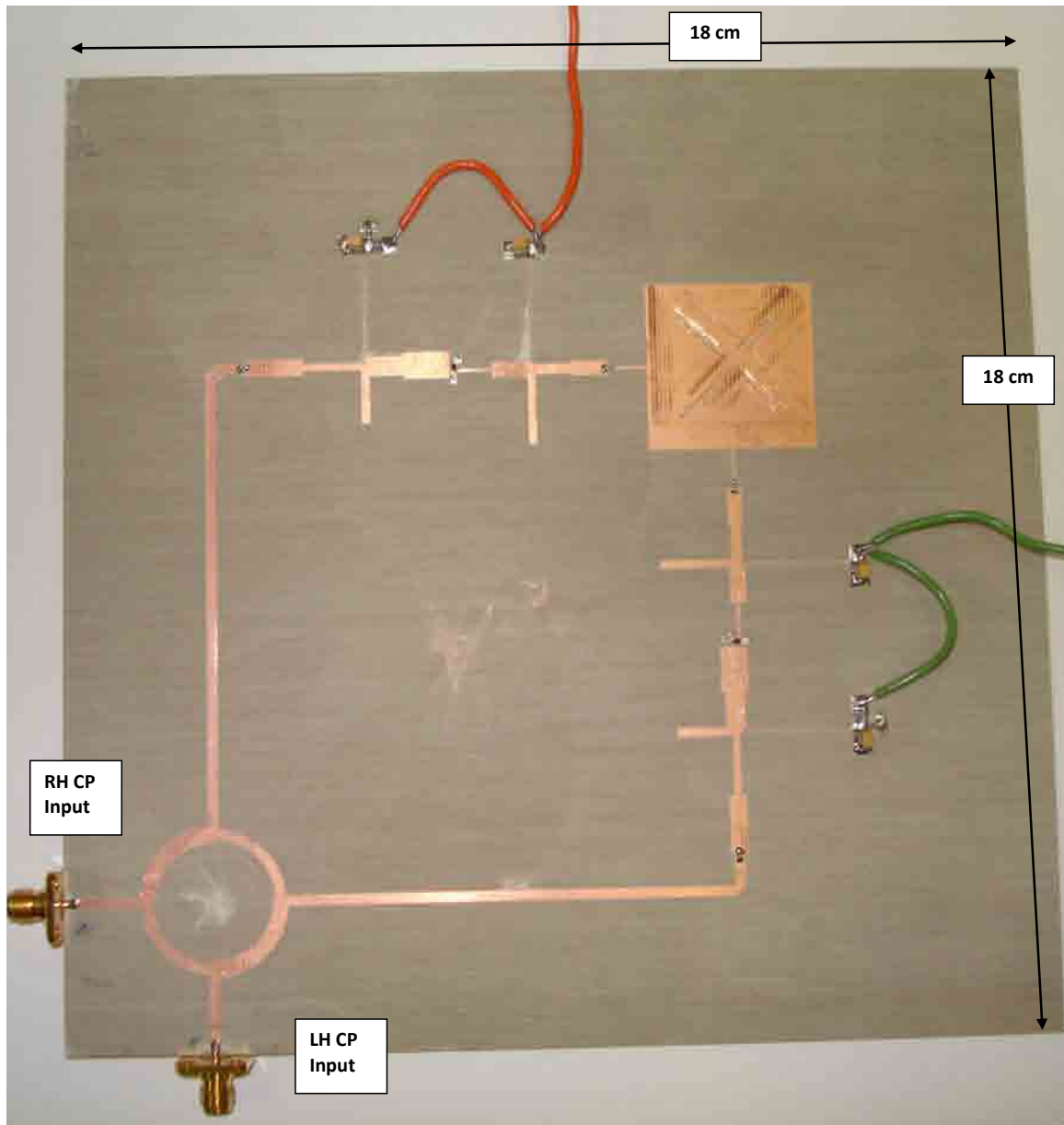e right-hand CP antenna, the co-polar component is the right-hand component and the cross-polar component is the left-hand component. Considering the difference between these two values as d in dB, Axial Ratio (AR) in dB is calculated using (5.1).

$$AR\ (dB) = 20\ log\left(\left(1 + 10^{d/20}\right) / \left(1 - 10^{d/20}\right)\right) \tag{5.1}$$

For example, $d = -15\ dB$ results in axial ratio of $AR = 3.12\ dB$ and for $d = -20\ dB$ it would be $AR = 1.74\ dB$. For AR less than $3\ dB$ criteria, the difference of $15\ dB$ between two components in the direction of maximum directivity is acceptable for the antenna to have circular polarization.

For each type of circular polarization the antenna was excited and co-polar and cross-polar components in two planes of $\Phi = 0°$ and $\Phi = 90°$ were measured and the results are compared with simulation shown in Fig. 5.9 and Fig. 5.10 for the right-hand circular polarization and in Fig. 5.11 and Fig. 5.12 for the left-hand circular polarization.

About $15\ dB$ difference between two co-polar and cross-polar components of radiation pattern is observed. There is a significant difference between simulation and measurement results of cross-polar component's levels which is due to the radiation effect of the rest of the circuit as explained in Chapter 4. Another important parameter in a CP antenna is to have the same magnitude for two excitations. The branch-line coupler is providing an equal power level for the amplifiers but there is a possibility of difference between amplifiers' gain because of tolerance in components as well as fabrication process. These could result in a difference in power level of the patch input ports which can affect the axial ratio for the circular polarization as can be seen in the radiation pattern plots.

Antenna's maximum directivity is being measured and it has $6.42\ dB$ directivity for right-hand circular polarization and $6.53\ dB$ for the left-hand circular polarization and we

Fig. 5.9: Radiation pattern of active integrated right-hand CP patch antenna at $2.4\,GHz$ in $\Phi = 0°$ cut.

Fig. 5.10: Radiation pattern of active integrated right-hand CP patch antenna at $2.4\,GHz$ in $\Phi = 90°$ cut.
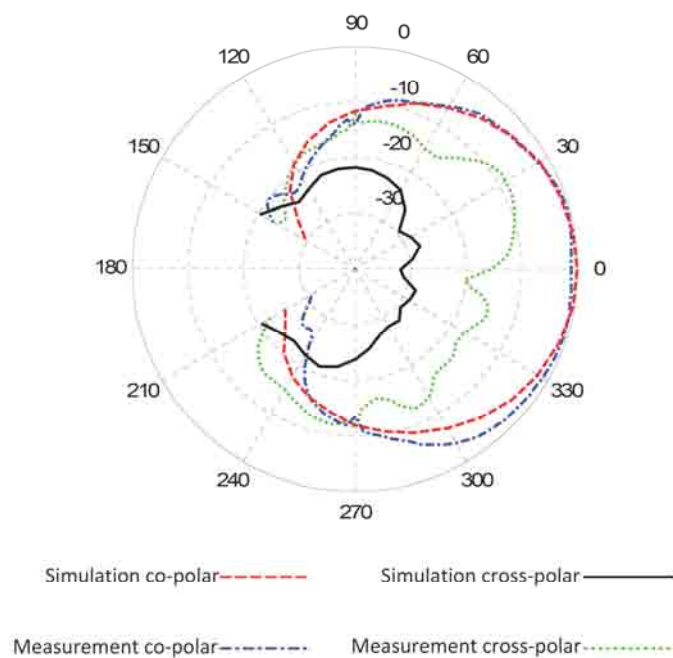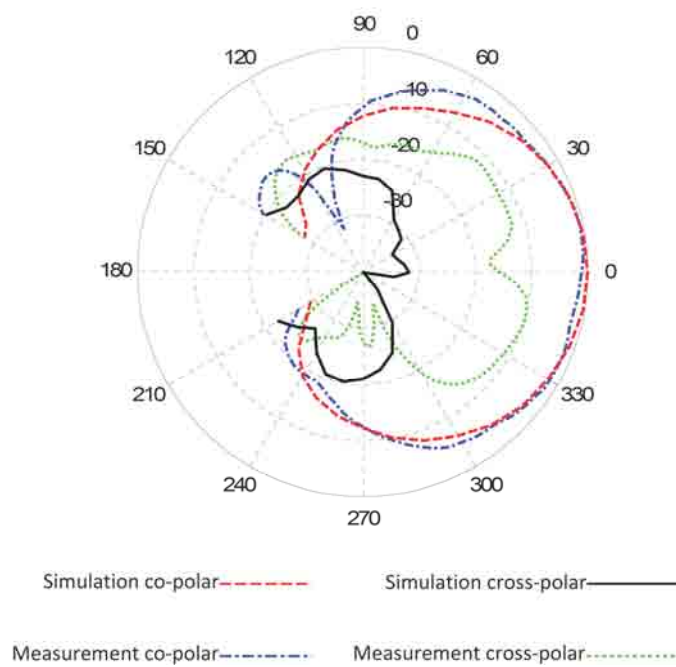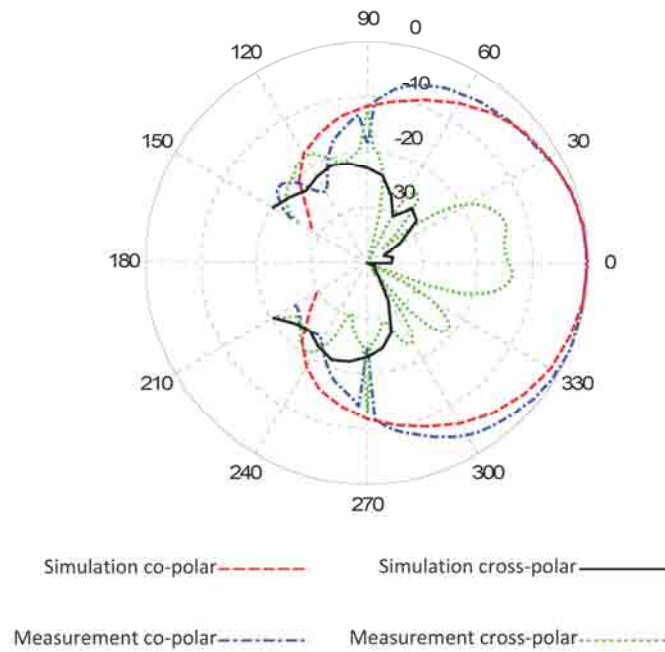
Fig. 5.11: Radiation pattern of active integrated left-hand CP patch antenna at $2.4\,GHz$ in $\Phi = 0°$ cut.
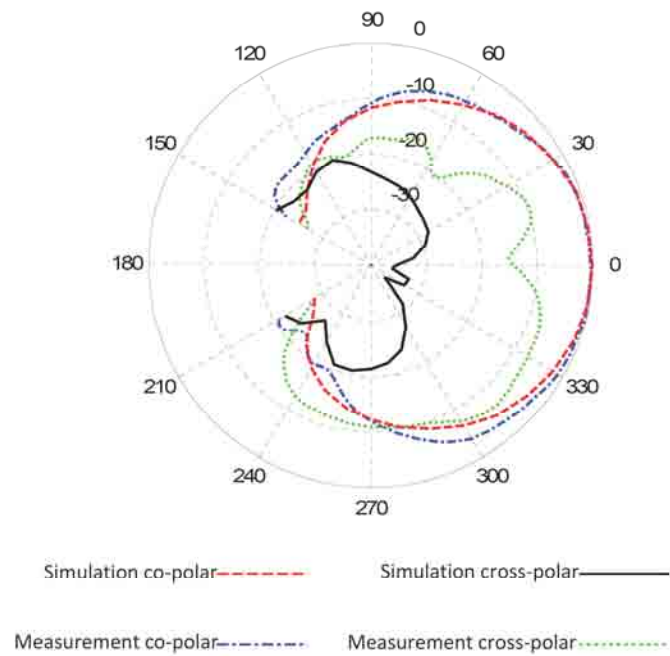
Fig. 5.12: Radiation pattern of active integrated left-hand CP patch antenna at $2.4\,GHz$ in $\Phi = 90°$ cut.

can see the patch antenna with harmonic suppression can be used as a CP antenna in an active circuit with an acceptable axial ratio.

Chapter 6

Feasibility Study for Future Work and Summary

6.1 Introduction

Having an active patch antenna that supports linear and circular polarization is a starting point for designing the antenna array with integrated active elements. An array antenna provides higher directivity and the ability of beam steering in scanning array antennas. This chapter presents a study on AIA in array configuration. All simulations were performed using HFSS and were based on the antenna structure with harmonic suppression without considering the amplifier's effects. Each integrated amplifier increases the input power level for every single patch and the total effect can be calculated in system level simulations.

6.1.1 An AIA Array with Linear Polarization

An array of five elements shown in Fig. 6.1 is an example to investigate the linear behavior of the structure. Each antenna has a single feed and the spacing between antenna elements is $d = \lambda/2$.

Fig. 6.1: Array of five elements for linear polarization.

In the first simulation, all elements were fed with the same magnitude and phase. The antenna radiates with 0 degrees beam tilting and maximum directivity of 11.36 dB. The 3-D pattern of directivity for this array is shown in Fig. 6.2. Radiation pattern of this array in two planes of $\Ph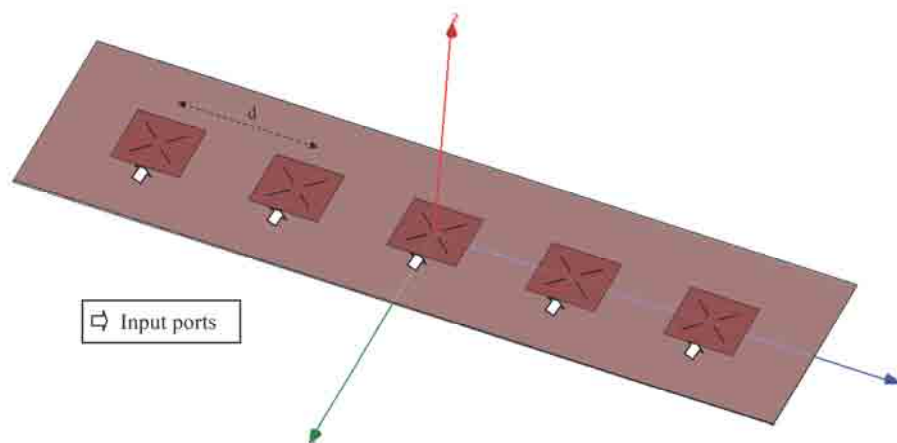i = 0°$ and $\Phi = 90°$ are shown in Fig. 6.3. Strong co-polar components compared with cross-polar components approve linear polarization in the array structure. Radiation of this array could be controlled by changing the amplitude or phase of each element as well as the spacing between them. Beam tilting by providing 90 degrees phase difference between every two elements is simulated and shown in Fig. 6.4 as an example. Other parameters might vary depends on the application for the antenna.

6.1.2 An AIA Array with Circular Polarization

An array of four elements (two by two), shown in Fig. 6.5, is another example to show circular polarization in the array structure. Every patch element is fed with two excitation ports and the spacing between them is $d = \lambda/2$ in both directions.

Feeding all elements with the same magnitude and phase results in broadside radiation. This phase is defined for the element and each element has two feeds which they have 90 degrees phase difference for right-hand CP excitation. The antenna radiates with 0 degrees beam tilting and maximum directivity of 11.55 dB. The 3-D pattern of directivity for this array is shown in Fig. 6.6.

Fig. 6.2: 3-D pattern of directivity for array of five elements 0 degrees beam tilting.

Fig. 6.3: Radiation patterns of array of five elements in two planes of $\Phi = 0°$ and $\Phi = 90°$ for linear polarization.
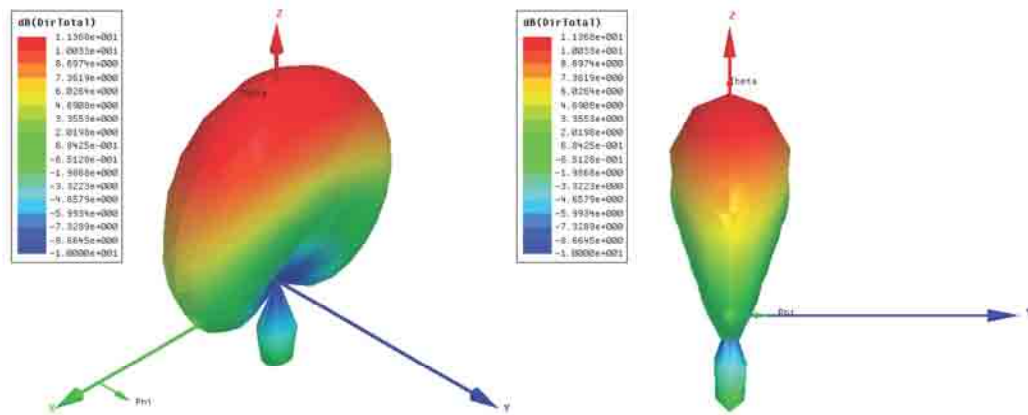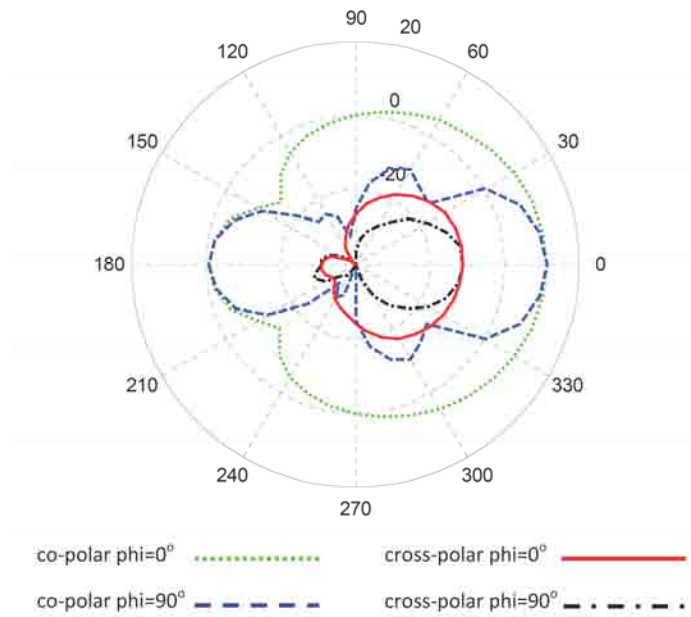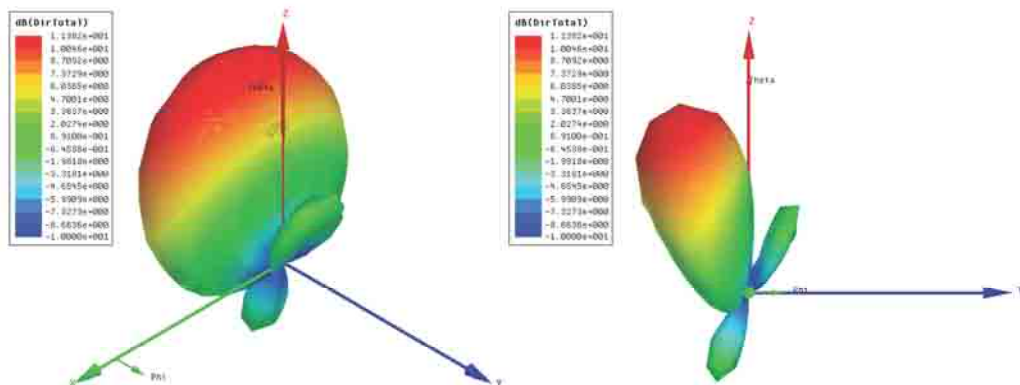

Fig. 6.4: 3-D pattern of directivity for array of five elements 30 degrees beam tilting.
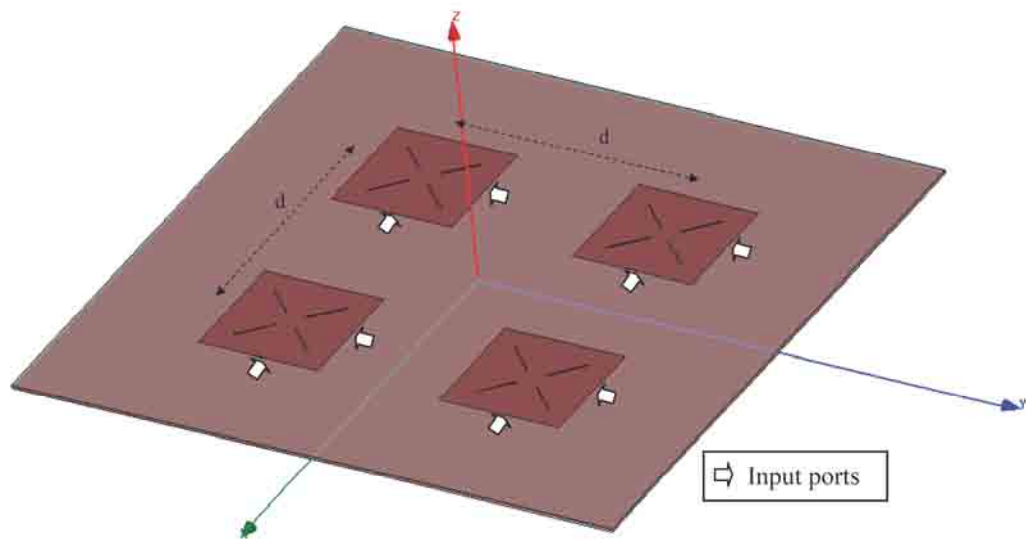
Fig. 6.5: Array of four elements for circular polarization.
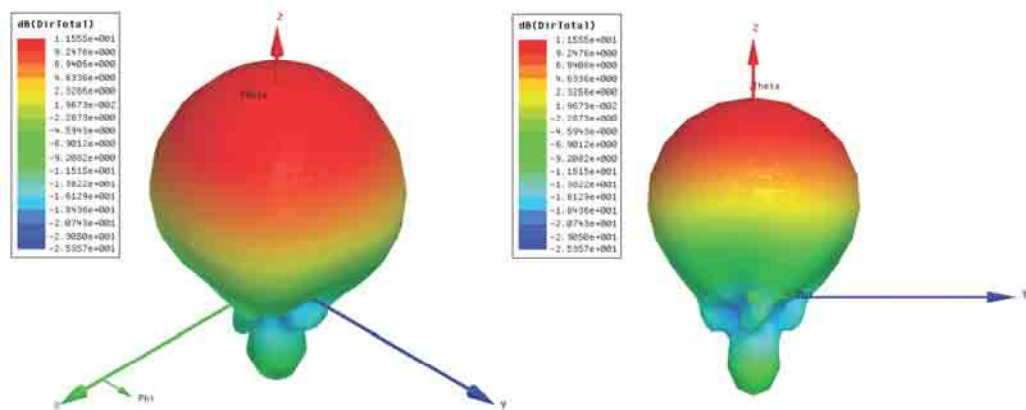
Fig. 6.6: 3-D pattern of directivity for array of four elements 0 degrees beam tilting.

The radiation pattern of this array in two planes of $\Phi = 0°$ and $\Phi = 90°$ are shown in Fig. 6.7. Strong co-polar components (right-hand CP) compared with cross-polar components (left-hand CP) approve circular polarization in the array structure.

6.2 Summary

In this thesis, we worked on active integration to the patch antenna with the goal of improvement in efficiency of the circuit as well as compactness of the RF front end module. This objective is achieved by implementing the novel harmonic suppression technique in the patch antenna, which is easy to fabricate compared with shorting pins structure and also compatible with all needed radiation polarizations required for satellite communication including linear and circular polarization.

The antenna design with harmonic suppressing capability was studied using HFSS, and the input impedance of the antenna is used as the load of the amplifier. The matching circuit for the amplifier was designed using ADS, and the final amplifier circuit was integrated with the patch antenna for linear polarization.

Fig. 6.7: Radiation patterns of array of four elements in two planes of $\Phi = 0°$ and $\Phi = 90°$ for circular polarization.

After fabricating the active antenna, the measurement for power added efficiency for the amplifier and radiation pattern of the antenna was performed inside the anechoic chamber using near field measurement equipment. Amplifier's output power was measured using the Friis transmission equation and the calibration for the measurement setup was required for accurate results.

The measurement results showed a good radiation pattern with linear polarization and power measurement agreed with $4-5\%$ improvement in the power added efficiency of the amplifier as was expected based on the ADS simulation results.
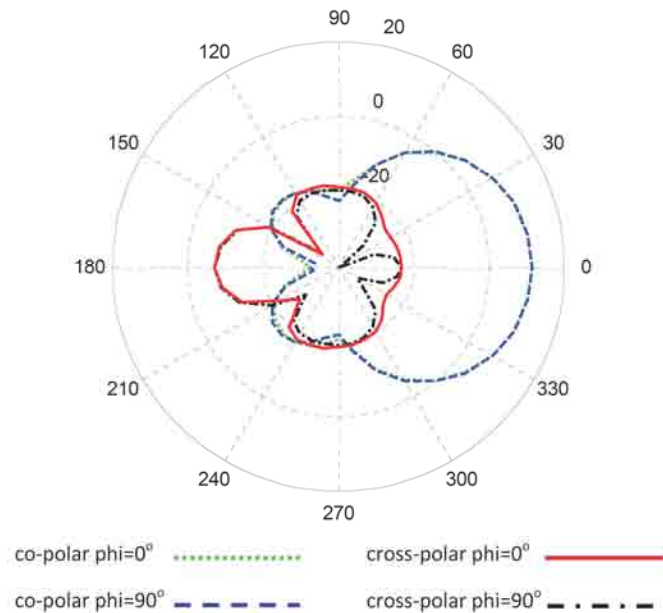
Finally, for the circular polarization, the antenna was excited with two orthogonal ports with the same power level and 90 degrees phase difference. This provides circular polarization for a symmetric square patch antenna. The power division and the phase difference was achieved by an integrated branch-line coupler in the circuit. Measurement results showed good axial ratio for both right-hand and left-hand circular polarizations.

The proposed active integrated antenna can be used as a single element or as an array of active patch elements. As showed in feasible study, it provides higher gain and efficiency in a system as a result of harmonic suppression. As the next step, one may prototype an array of AIA and measure the improved PAE of the entire array. The measurement method can be the same as outlined in Chapter 4. As a future work, one may implement Monolithic Microwave Integrated Circuits (MMIC) or Micro Electro Mechanical Systems (MEMS) to control both phase and amplitude of an AIA scanning array. Using low-power elements to get high transmit power with less loss and price may become an alternative for high-power amplifiers and parabolic antennas in the future, making it possible to replace bulky systems with much lighter and cheaper planar array.

References

[1] V. Radisic, Y. Qian, and T. Itoh, "Novel architectures for high-efficiency amplifiers for wireless applications," *Microwave Theory and Techniques, IEEE Transactions*, vol. 46, no. 11, pp. 1901–1909, Nov. 1998.

[2] K. Chang, R. York, P. Hall, and T. Itoh, "Active integrated antennas," *Microwave Theory and Techniques, IEEE Transactions*, vol. 50, no. 3, pp. 937–944, Mar. 2002.

[3] S. Lucyszn, "Power-added efficiency errors with RF power amplifiers," *International Journal of Electronics*, vol. 82, pp. 303–312, Mar. 1997.

[4] Y. Qian and T. Itoh, "Progress in active integrated antennas and their applications," *Microwave Theory and Techniques, IEEE Transactions*, vol. 46, no. 11, pp. 1891–1900, Nov. 1998.

[5] D. Goshi, K. Leong, and T. Itoh, "Electronics insertion into printed antennas," in *Antennas and Propagation, 2006. EuCAP 2006. First European Conference*, pp. 1–4, Nov. 2006.

[6] H. Kim and Y. J. Yoon, "Wideband design of the fully integrated transmitter front-end with high power-added efficiency," *Microwave Theory and Techniques, IEEE Transactions*, vol. 55, no. 5, pp. 916–924, May 2007.

[7] H. Kim, I.-J. Yoon, and Y. J. Yoon, "A novel fully integrated transmitter front-end with high power-added efficiency," *Microwave Theory and Techniques, IEEE Transactions*, vol. 53, no. 10, pp. 3206–3214, Oct. 2005.

[8] W. Deal, V. Radisic, Y. Qian, and T. Itoh, "Integrated-antenna push-pull power amplifiers," *Microwave Theory and Techniques, IEEE Transactions*, vol. 47, no. 8, pp. 1418–1425, Aug. 1999.

[9] C. Hang, W. Deal, Y. Qian, and T. Itoh, "Push-pull power amplifier integrated with microstrip leaky-wave antenna," *Electronics Letters*, vol. 35, no. 22, pp. 1891–1893, Oct. 1999.

[10] C. Hang, W. Deal, Y. Qian, and T. Itoh, "High-efficiency push-pull power amplifier integrated with quasi-Yagi antenna," *Microwave Theory and Techniques, IEEE Transactions*, vol. 49, no. 6, pp. 1155–1161, June 2001.

[11] L. Chiu, T. Yum, C. Chin, Q. Xue, and C. Chan, "High-efficiency class-B push-pull amplifying array for microwave transmitting front end," *Microwaves, Antennas and Propagation, IEE Proceedings*, vol. 153, no. 1, pp. 25–28, Feb. 2006.

[12] J.-Y. Park, S.-M. Han, and T. Itoh, "A rectenna design with harmonic-rejecting circular-sector antenna," *Antennas and Wireless Propagation Letters, IEEE*, vol. 3, pp. 52–54, Dec. 2004.

[13] S. Al-Shahrani, *Design of Class-E Radio Frequency Power Amplifier*. Ph.D. dissertation, Virginia Polytechnic Institute and State University, Blacksburg, VA, 2001.

[14] I. Bahl, *Fundamentals of RF and Microwave Transistor Amplifiers*.   Hoboken, NJ: John Wiley and Sons, 2009.

[15] G. Gonzalez, *Micrownve Transistor Amplifiers*.   Englewood Cliffs, NJ: Prentice Hall, 1984.

[16] D. M. Pozar, *Micrownve Engineering*.   Hoboken, NJ: John Wiley and Sons, 2005.

[17] California Eastern Laboratories, [www.cel.com].

[18] Agilent Technologies, [www.agilent.com].

[19] Rogers Corporation, [www.rogerscorp.com].

[20] AutoCAD, [www.autodesk.com].

[21] Epoxy Technology, [www.epotek.com].

[22] S. F. Ooi, S. K. Lee, A. Sambell, E. Korolkiewicz, and S. Scott, "A new approach to the design of a compact high efficiency active integrated antenna," *Microwave and Optical Technology Letters*, vol. 50, no. 3, pp. 585–589, Mar. 2008.

[23] D.-H. Choi, Y.-J. Cho, and S.-O. Park, "A broadband slot antenna with harmonic suppression," *Microwave and Optical Technology Letters*, vol. 48, no. 10, pp. 1984–1987, Oct. 2006.

[24] H. Kim and Y. J. Yoon, "Microstrip-fed slot antennas with suppressed harmonics," *Antennas and Propagation, IEEE Transactions*, vol. 53, no. 9, pp. 2809–2817, Sept. 2005.

[25] V. Radisic, S. T. Chew, Y. Qian, and T. Itoh, "High-efficiency power amplifier integrated with antenna," *Microwave and Guided Wave Letters, IEEE*, vol. 7, no. 2, pp. 39–41, Feb. 1997.

[26] P. Colantonio, F. Giannini, E. Limiti, and G. Marrocco, "A method for PA-patch antenna design optimisation oriented to maximum efficiency," in *12th GAAS Symposium, Amsterdam*, pp. 25–28, Oct. 2004.

[27] Y. Chung, C. Hang, S. Cai, Y. Qian, C. Wen, K. Wang, and T. Itoh, "AlGaN/GaN HFET power amplifier integrated with microstrip antenna for RF front-end applications," *Microwave Theory and Techniques, IEEE Transactions*, vol. 51, no. 2, pp. 653–659, Feb. 2003.

[28] V. Radisic, Y. Qian, and T. Itoh, "Class F power amplifier integrated with circular sector microstrip antenna," in *Microwave Symposium Digest, 1997. IEEE MTT-S International*, vol. 2, pp. 687–690, June 1997.

[29] J. Fredrick and T. Itoh, "Recent developments in RF front ends based upon active antenna concepts," in *Telecommunications in Modern Satellite, Cable and Broadcasting Service, 2001. TELSIKS 2001. 5th International Conference*, vol. 1, pp. 3–9, Sept. 2001.

[30] S. Kwon, B. M. Lee, Y. J. Yoon, W. Y. Song, and J.-G. Yook, "A harmonic suppression antenna for an active integrated antenna," *Microwave and Wireless Components Letters, IEEE*, vol. 13, no. 2, pp. 54–56, Feb. 2003.

[31] C. I. Lee, W. C. Lin, Y. T. Lin, and Y. T. Lee, "A novel H-shaped slot-coupled antenna for the integration of poweramplifer," in *Progress In Electromagnetics Research Symposium Proceedings*, pp. 385–389, July 2010.

[32] V. Radisic, Y. Qian, and T. Itoh, "Broadband power amplifier integrated with slot antenna and novel harmonic tuning structure," in *Microwave Symposium Digest, 1998 IEEE MTT-S International*, vol. 3, pp. 1895–1898, June 1998.

[33] V. Radisic, Y. Qian, and T. Itoh, "Broad-band power amplifier using dielectric photonic bandgap structure," *Microwave and Guided Wave Letters, IEEE*, vol. 8, no. 1, pp. 13–14, Jan. 1998.

[34] C. Hang, Y. Qian, and T. Itoh, "High efficiency S-band class AB push-pull power amplifier with wideband harmonic suppression," in *Microwave Symposium Digest, 2001 IEEE MTT-S International*, vol. 2, pp. 1079–1082, June 2001.

[35] Y. Horii and M. Tsutsumi, "Harmonic control by photonic bandgap on microstrip patch antenna," *Microwave and Guided Wave Letters, IEEE*, vol. 9, no. 1, pp. 13–15, Jan. 1999.

[36] F.-R. Yang, K.-P. Ma, Y. Qian, and T. Itoh, "A uniplanar compact photonic-bandgap (UC-PBG) structure and its applications for microwave circuit," *Microwave Theory and Techniques, IEEE Transactions*, vol. 47, no. 8, pp. 1509–1514, Aug. 1999.

[37] Y. Sung and Y.-S. Kim, "An improved design of microstrip patch antennas using photonic bandgap structure," *Antennas and Propagation, IEEE Transactions*, vol. 53, no. 5, pp. 1799–1804, May 2005.

[38] Y. Sung, M. Kim, and Y. Kim, "Harmonics reduction with defected ground structure for a microstrip patch antenna," *Antennas and Wireless Propagation Letters, IEEE*, vol. 2, no. 1, pp. 111–113, Dec. 2003.

[39] H. Kim and Y. J. Yoon, "Compact microstrip-fed meander slot antenna for harmonic suppression," *Electronics Letters*, vol. 39, no. 10, pp. 762–763, May 2003.

[40] C. A. Balanis, *Antenna Theory, Analysis, and Design.* Hoboken, NJ: John Wiley and Sons, 2005.

[41] K. Hirasawa and M. Haneishi, *Analysis, Design, and Measurement of Small and Low-Profile Antennas.* Norwood, MA: Artech House, 1991.

[42] P. Bhartia, K. V. S. Rao, and R. S. Tomar, *Millimeter-Wave Microstrip and Printed Circuit Antennas.* Norwood, MA: Artech House, 1991.

[43] R. Bancroft, *Microstrip and Printed Antenna Design.* Atlanta, GA: Noble Publishing, 2004.

[44] ANSYS, Inc., [www.ansys.com].

[45] Nearfield Systems Inc., [www.nearfield.com].